A FLOW VISUALIZATION STUDY OF A HIGH PITCH CYCLOIDAL PROPELLER

Alfred L. Jobst, et al

Engineering Research Associates

Prepared for:

Naval Ship Research and Development Center

August 1972

ERA REPORT NO. 60 - 2

ERA

A FLOW VISUALIZATION STUDY OF A HIGH PITCH CYCLOIDAL PROPELLER

A. L. Jobst

P. A. Bandler

August 1972

This research was carried out under the
Naval Ship System Command
General Hydromechanics Research Program
Sub project SR 009 01 01, administered by the
Naval Ship Research and Development Center
ONR Contract N00014 - 66 - C0191

Approved for publication; distribution unlimited

ENGINEERING RESEARCH ASSOCIATES
160 BAY STREET TORONTO CANADA

Unclassified

Security Classification

DOCUMENT CONTROL DATA - R & D

(Security classification of title, body of abstract and indexing annotation must be entered when the overall report is classified)

1. ORIGINATING ACTIVITY (Corporate author)

Engineering Research Associates
160 Bay Street, Toronto 1, Canada

2a. REPORT SECURITY CLASSIFICATION

Unclassified

2b. GROUP

3. REPORT TITLE

A FLOW VISUALIZATION STUDY OF A HIGH PITCH CYCLOIDAL PROPELLER

4. DESCRIPTIVE NOTES (Type of report and inclusive dates)

Final Report

5. AUTHOR(S) (First name, middle initial, last name)

Alfred L. Jobst
Peter A. Bandler

6. REPORT DATE: August 1972

7a. TOTAL NO. OF PAGES: 58

7b. NO. OF REFS: 4

8a. CONTRACT OR GRANT NO.: N00014 - 66 - C0191

b. PROJECT NO.: SR 009 01 01

c.

d.

9a. ORIGINATOR'S REPORT NUMBER(S): 60 - 2

9b. OTHER REPORT NO(S) (Any other numbers that may be assigned this report)

10. DISTRIBUTION STATEMENT

This document has been approved for public release and sale; its distribution is unlimited.

11. SUPPLEMENTARY NOTES

Details of illustrations in this document may be better studied on microfiche.

12. SPONSORING MILITARY ACTIVITY

Naval Ship Research and Development Center
Department of the Navy, Washington D. C. 20007

13. ABSTRACT

An experimental test program designed to study the flow through a cycloidal propeller ($P/D = \pi/.70$) was conducted in the water tunnel at the National Research Laboratories in Ottawa.

Visualization of the flow was achieved by injecting reflecting particles that followed the streamlines and by illuminating sections of the flow with a plane light source. Records were made using both still and movie cameras.

The tunnel speed was varied to permit views of the working model to be taken at several advance ratios. For purposes of detailed analysis, the actual angle of attack and resultant velocity vectors were calculated from the inflow parameters obtained from still pictures. The loads normal to the blade were measured and compared to loads obtained by calculation.

DD FORM 1 NOV 65 1473

Unclassified

Security Classification

ENGINEERING RESEARCH ASSOCIATES

ERA REPORT NO. 60 - 2

A FLOW VISUALIZATION STUDY OF A HIGH PITCH CYCLOIDAL PROPELLER

A. L. Jobst

P. A. Bandler

August 1972

This research was carried out under the
Naval Ship System Command
General Hydromechanics Research Program
Sub project SR 009 01 01, administered by the
Naval Ship Research and Development Center
ONR Contract N00014 - 66 - C0191

ABSTRACT

This is a presentation of a study on a cycloidal propeller with a pitch ratio of $\pi/.70$. The inflow parameters are determined by flow visualization techniques over a full orbital cycle for various advance ratios. The flow parameters are used to calculate blade loads and are compared to loads measured by load transducers. The test results are finally compared with the results of a test with a cycloidal propeller having a pitch ratio of $.70\pi$.

TABLE OF CONTENTS

LIST OF FIGURES

LIST OF SYMBOLS

A	Blade Area, $L\bar{c}$	ft^2
AR	Aspect Ratio, $\frac{2L}{\bar{c}}$	-
BAR	Blade Area Ratio, $\frac{(\text{No. of Blades})A}{LD}$	-
$\bar{c}$	Average Blade Chord	ft
C_{L_α}	Lift Curve Slope	rad^{-1}
D	Orbital Diameter	ft
J	Advance Ratio, $\frac{V_o}{nD}$	-
K_T	Thrust Coefficient	-
L	Blade Length	ft
n	Rotational Speed	rps
P	Propeller Pitch, $\frac{V}{n}$	ft/rev
R	Orbital Radius	ft
R_n	Reynolds Number, $\frac{\bar{c}\sqrt{V_o^2 + (R\Omega)^2}}{\nu}$	-
T	Thrust	lb
V	Velocity at 'Zero Slip'	ft/sec

V_o	Free Stream Velocity	ft/sec
V_i	Inflow Velocity	ft/sec
$\overline{V}_{ideal}$	Resultant Velocity - ideal, $\sqrt{V_o^2 + (R\Omega)^2 + 2V_o R\Omega \cos\theta}$	ft/sec
$\overline{V}$	Resultant Velocity, $\sqrt{V_i^2 + (R\Omega)^2 + 2V_i R\Omega \cos\theta}$	ft/sec
x/L	Fraction of Span Relative to the Root	-
α	Angle of Attack	deg
α_{ideal}	Angle of Attack - ideal	deg
$\Delta\alpha$	Deviation from the Ideal Angle of Attack, $\alpha_{ideal} - \alpha$	deg
β	Blade Angle	deg
θ	Rotation Angle - $\theta = 90°$ is Ahead	deg
ϕ	Inflow Angle	deg
Ω	Angular Velocity	rad/sec
ρ	Density	lb sec^2 / ft^4
ν	Kinematic Viscosity	ft^2 /sec

1.0 INTRODUCTION

A program of research and development for the cycloidal propeller was formulated in the Bureau of Ships, Navy Department in 1958 . In 1965, John McKillop of ERA devised and implemented an experimental study, designed to gain a visual insight into the nature of the flow through a propeller.

A small working model with a pitch ratio of $.70\pi$ was placed in a water tunnel. A motion picture record was made in which the flow was observed from three different viewpoints. General flow pictures were taken with the camera stationary. Then the camera was made to rotate and follow the orbit of a blade, recording the motion of the blade about its pitch axis and the flow relative to the rotating disc. Finally the camera was made to rotate and also follow the pitching motion of the blade, illustrating the flow relative to the blade chord. Still pictures were taken to obtain the inflow vectors, from which the resultant velocity vector and the blade angle of attack were calculated over the full cycle. The blade load time history was calculated and compared to a measured blade load time history.

The technique offers promise for further studies and accordingly the model was modified to a pitch ratio of $\pi/.70$. This is a relatively high pitch ratio which could find application in a high speed craft. The present study essentially follows along the lines of the earlier experimental program.

Regrettably it must be recorded that John lost his life while engaged in a test flight, an event of sadness for his friends and colleagues. He had made good progress in the present study, which was completed by the present author.

2.0 GEOMETRY AND FLOW PARAMETERS

The cycloidal propeller achieves propulsive thrust through the rotation of wing-like blades in an orbital circle and by controlling the attitude of the blades in a programmed manner. In the case of a pure cycloidal propeller the chord through the pitch axis is at all times normal to the line joining the pitch axis and a characteristic point, called the control center. In order to satisfy this requirement, the blade maintains a continuous pitching motion through the orbital cycle. A very sudden change in the blade attitude occurs in the region where the orbital path is closest to the control center.

The propeller pitch (P) is defined as the ratio of forward velocity at the "zero slip" condition, to the rate of rotation (V/n). At zero slip, the blade chord is parallel to the flight path and no lift is generated. In terms of geometry, the propeller pitch is $P = 2\pi X R$, where X expresses the distance from the center of rotation to the control center as a fraction of R. In this report, the propeller configuration will be characterized in terms of the non-dimensional pitch ratio ($P/D = X\pi$).

Figure 1 shows a sketch of a low and high pitch ratio propeller. The characteristic motion of the blade changes once the control center falls outside the orbital circle - pitch ratio greater than π. As long as the pitch ratio is less than π, the blade pitch alternates, as shown in the blade angle β diagram in Figure 1. Once the pitch ratio is greater than π, the blade pitches continuously against the direction of rotation.

The ideal flow parameters and geometry of a propeller of pitch ratio $\pi/.70$

are shown below. The cam tracks that control the blade pitch on the test model are also shown.

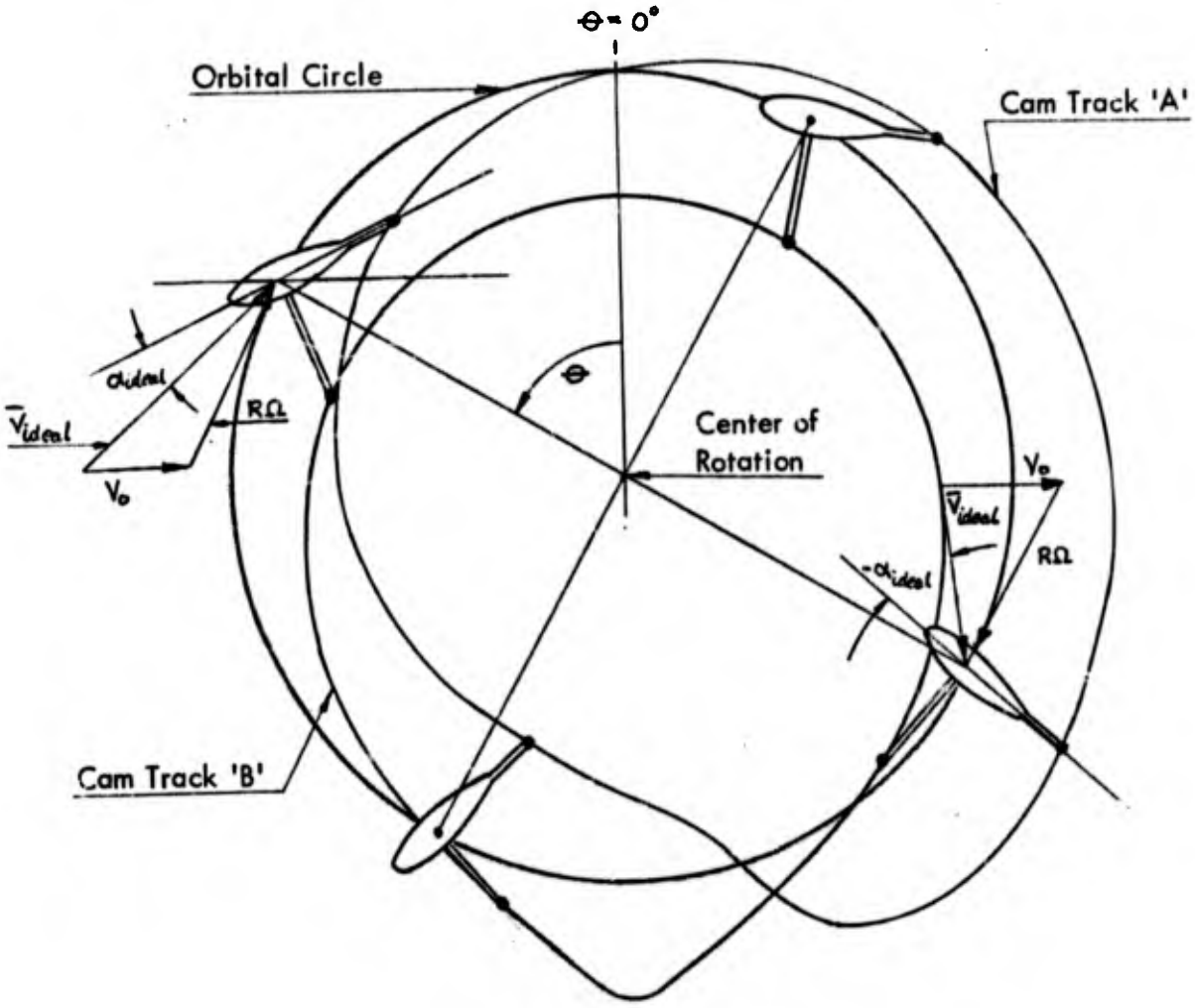

The vector diagram shows that the free stream velocity (V_o) and the rotational velocity ($R\Omega$) form the resultant vector ($\bar{V}_{ideal}$), which will give the blade an effective angle of attack α_{ideal} . This represents a theoretical condition. In actuality, the free stream velocity will be modified by the contraction of the flow

entering the propeller and by three-dimensional effects due to spanwise flow.

Figure 2 shows the cyclical variation of the angle of attack and velocity ratio, assuming the flow to be ideal - an undisturbed inflow over the complete cycle. The discontinuity in the angle of attack at $\theta = 180°$ indicates reverse flow on the blade, a condition which will exist until V_o is greater than $R\Omega$. The large angle of attack at low advance ratio is an indication of the inefficiency of the operation at low rates of advance. As the advance ratio is increased, the angle of attack decreases to the point where it becomes zero - the zero slip condition.

3.0 DESCIPTION OF THE TEST EQUIPMENT

3.1 The Model

A sturdy U-shaped frame houses the drive mechanism and supports the propeller disc assembly and the camera carrier.

The propeller assembly is shown fixed to the frame in Figure 3. The four blades rotate in an orbital circle 6.3" in diameter. A crank arm, fixed to the shaft of each blade, follows dual cams to generate the pitching motion. The cam tracks are shown on page 3.

The blades, Figure 4, are designed to a 0.70 scale of the rectangular blade used in Reference 2. The planform and dimensions are given in Figure 5.

One of the blades is instrumented with a semi-conductor load transducer, to measure the load over the cycle. Semi-conductors are required to give sufficient sensitivity to measure the small loads generated. The circuit is wired as a half-bridge and measures shear (lift forces) normal to the blade chord. Two slip rings

transmit the signal through the disc assembly.

In the side view of the model, Figure 6, the disc housing is seen facing the camera carrier. A counterweight that offsets the centrifugal forces generated by the camera and its carrier is housed on the opposite side of the frame. The motor is geared to a horizontal shaft, which then drives one chain to rotate the propeller disc and another similar chain to rotate the shaft connecting the camera and counter - weight assemblies.

Two modes of camera motion are possible. In either case, the camera lens is aligned with the pitch axis of one blade. In the articulated mode, the camera carrier is guided by a crank arm and cams to follow identically the rotational and pitching motion of the blade. The counterweight is similarily guided, but 180° out of phase. The camera is triggered by a solenoid switch. By removing one screw, the camera carrier can be disconnected from the cam system, to operate in the rotating mode.

In the articulated mode, the view is that of an observer located on the blade. In the rotating mode, the observer follows the orbital path, and also observes the pitching motion of the blade.

3.2 The Water Tunnel

The closed return water tunnel facility at the National Research Council laboratories in Ottawa has a working section 10" wide, 13" high and 32" long. The tunnel can be operated at variable velocities up to 10 feet per second.

A plane light source is located underneath the glass floor of the working section and operates on alternating current of 60, 120 or 180 cycles per second, so that the particles in the flow are illuminated 120, 240 or 360 times per second. The lamp is

used to illuminate two-dimensional sections in the direction of the flow, or it may be swung to throw its light across the flow. In the latter position a cross section through the propeller is viewed in the mirror placed obliquely downstream from the working section. Figure 7 shows the model installed in the tunnel. The propeller disc is inserted through an opening in the rear wall.

3.3 Flow Visualisation And Camera Technique

The visualisation is accomplished by highly reflective aluminum powder suspended in the flow. The paticles are light and follow the streamlines well. In order to view different sections along the span of the blades, the light plane is moved to the desired location. The flow can be observed visually through the front wall glass and recored by cameras. Since the blades are made of plexiglass, there are no regions that are obscured.

A Bolex 16 mm movie camera with a 25 mm, f 1.8 lens was used in the camera carrier and also for general viewing a 35 mm Leica M3, with a 90 mm, f 2.0 lens was used for still pictures.

Stills with a relative long exposure time define the stream lines which show as a series of dots. The steady flashing of the lamp provides a time source. Thus, upon measuring direction and length, the flow vectors are defined. This kind of record is used mainly to determine the inflow vectors.

Short exposure stills, where the particle is only seen once, are used to study the vortices within the overall flow.

Motion pictures are taken with the camera aticulated, rotating and stationary. The frame rate is varied depending on the desired effect. Slow motion is best

for direct viewing.

Selecting a frame rate which gives a reasonable stream line length provides an inexpensive method for detail studies. The negative can be used in a microfilm copy machine to give an enlargement clear enough to define the flow vector and blade geometry.

4.0 THE TEST PROGRAM

The performance of the test program required the simultaneous operation of the model, water tunnel, photographic equipment or blade load recorders. In order to test at four chosen advance ratios, the model was operated at 60 rpm and the free stream velocity was varied as follows:

V_o	J	$V_o/\pi nD$
0.28	0.56	0.18
0.92	1.75	0.56
1.83	3.50	1.11
2.36	4.50	1.43

The two higher advance ratios were chosen because they represent the zero slip condition ($J = 4.50$) and the region of maximum efficiency ($J = 3.50$). For purposes of continuity and comparison with the former test, the two lower conditions were included.

At each speed the lamp was moved to illuminate the blade at four span locations namely at the tip and 75, 50, 25 percent of the span.

Pictures of the spanwise sections of the general flow were taken with the 35 mm still camera. The lamp rate was 240 flashes per second and various exposure times were used to obtain well defined streamlines on the photo records.

Stills were also taken through cross-sections of the propeller, at the center line and the rear radius (Reference 1, page 7) . These pictures show the crossflow that exists along the blades.

The motion pictures were taken with the fixed camera, rotating and articulated camera. Frame rates were varied from 12 to 64 frames per second. The high frame rate is best for direct viewing, since it slows down the motion, but even so, events pass quite quickly. For this reason an additional viewing technique was employed. Single frames with stream line effects were duplicated, so that the same frame is seen for approximately one second. The blade is seen at one location for some time and then the process is repeated a step further in the cycle, to give a 'stopped motion' effect. The movie footage was assembled into a film, auxiliary to this report.

An attempt was made to evaluate the flow relative to the blade using enlargements from the 16 mm negative. A microfilm copy machine magnified the frames taken by the articulated camera. The resultant velocity agreed well with the calculated dato; however the backlash in the drive system prevented the accurate determination of the angle of attack.

The blade loads were measured for the same advance ratios as the flow data. A load transducer was calibrated before and after the test, over the full range of expected loads. In addition, one point was checked throughout the duration of the test using a calibration resistor . The inertia forces and the natural frequency of the blade were also measured and applied to correct the load data. To insure the repeatability of the loads records, the test program was performed several times.

5.0 ANALYSIS AND DISCUSSION OF THE TEST RESULTS

5.1 The Flow Data

The inflow velocity and inflow angle were obtained from the long exposure stills taken of the general flow, and are presented in graphical form to depict the variation over the disc perimeter. These data were then used to carry out discrete calculations at 30° intervals to evaluate the resultant inflow velocity and actual angle of attack.

In the sketch below the theoretical and actual flow vectors on a blade are shown with the nomenclature used.

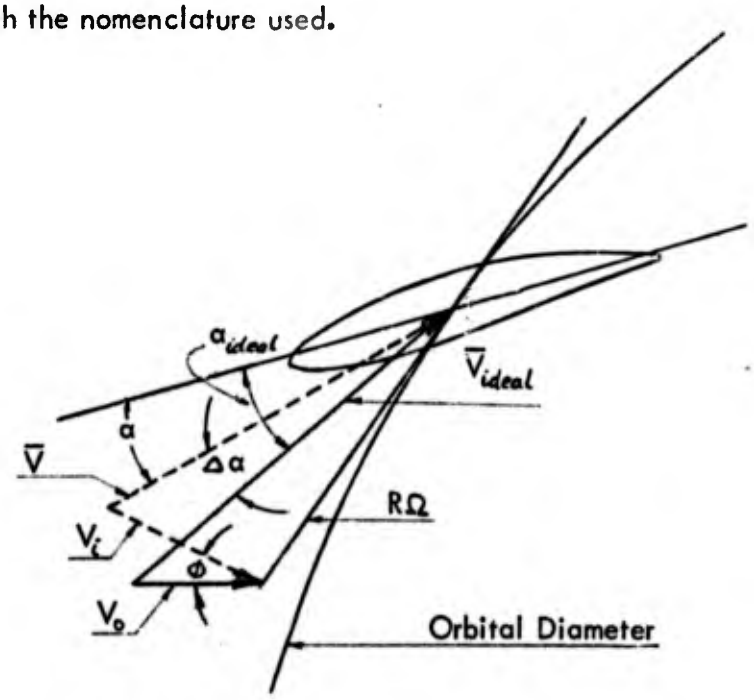

The solid vector diagram represents the ideal flow, the broken lines represents the flow modified by the inflow effect. Δa is the difference between the ideal and the actual angle of attack.

Typical photographs used for the flow analysis are shown in Figures 14 to 17 . The sections shown are taken at mid-span of the blade for the advance ratios J = 0.56, 1.75, 3.50 and 4.50 . The flow is entering the propeller from the left and the propeller is rotating counter clockwise.

At the lowest advance ratio (J = 0.56, Figure 14), the flow in the region $\theta = 270°$ to 45° is extremely disturbed. This effect was already observed in the former tests but is more pronounced in the higher pitch ratio test. It can be seen that it is the result of an interaction between the vortex sheet behind the blade and the free stream flow. The free vortex leaving the trailing edge of the blade rotates counter clockwise, while the bound vortex rotates clockwise. The two are so strong that they curve the flow and in some regions bring it to a complete standstill. The same effect exists at the higher advance ratios, but it is not so clearly visible. The best view of the effect can be seen in the motion picture.

At J = 1.75, Figure 15, another typical effect is seen, namely the disturbed regions caused by the blade on the forward cycle ($\theta = 0°$ to 180°). These disturbances travel aft and are encountered by the blades on the return cycle ($\theta = 180°$ to 360°).

On reaching the region of maximum efficiency (J = 3.50, Figure 16), the flow has become quite smooth because of the high free stream velocity. At the zero slip condition (J = 4.50), the flow passes through the propeller without any modification.

The results of these general flow pictures are plotted in Figures 8, 10 and 12 . The inflow velocity is normalized over the free stream velocity. The deviation from the ideal flow is greatest at the low advance ratios, at which the flow ex-

periences the highest accelerations due to the concentration of the inflow towards the center of the propeller disc. It has to be recognized that the data has a certain scatter, but nervertheless the trends are evident.

The calculated angles of attack and the resultant velocity ratios are shown on Figures 9, 11 and 13 . For J = 0.56 and J = 1.75 the angle of attack reaches such high values that the difference from the ideal values is not significant enough to show the variation; to improve the presentation, the difference between the ideal and the actual angle of attack is shown ($\Delta\alpha$) . The actual α can be obtained by adding $\Delta\alpha$ to α_{ideal} . J = 0.56 (Figure 9) shows quite a scatter and deviation from the ideal. Figure 11 shows the trend for J = 1.75 . Here the velocity is well behaved, though slightly increased on the return cycle due to energy added by the blade. There is a slight variation across the span with the flow at the tip behaving closest to the ideal flow.

The advance ratio giving the maximum efficiency is presented in Figure 13 . The smooth flow, observed on the pictures, causes very small variations in the resultant velocity. But the angle of attack is now small and is sensitive to relatively small velocity changes, as one can deduce from the vector diagram on page 9 . On the return cycle there is still a considerable reduction in α. The values around $\theta = 180°$ are not shown since this region is largely influenced by the vortex due to the sudden blade pitch. An interesting observation is that the angle of attack has a small variation over the span, contrary to the results of the low pitch propeller test.

Another conclusion, to be drawn from Figure 9, is that the pure cycloidal propeller does not give the highest possible lift. It seems that in the regions

θ = 40° to 100° and θ = 260° to 320° a higher angle of attack could be tolerated, especially since it would coincide with a high resultant velocity. Although the thrust would probably show a high variation over the cycle, it would still result in a net increase.

In Figures 18 to 21 transverse sections of the propeller are shown, viewed from the downstream side (J = 0.56 and J = 3.50). At the lower advance ratio, large span-wise flow components exist from the tip to about 50% span. The centerline section, Figure 18, also shows the flow around θ = 0° drifting towards the center of the disc, as already observed in the general flow pictures. At the higher advance ratio the flow is quite uniform and consistent with the general flow pictures.

For detail flow studies, sequence pictures over a full cycle, are taken with a 16mm movie camera and some enlargements are shown in Figures 22 to 29. In the sequences taken with the camera fixed, Figures 22 and 23, the flow is similar to the general flow pictures already discussed. The frames using the rotating camera, Figures 24 and 25, show the cycloidal effect. Figure 26 to 29 show a blade over the full cycle, taken with the articulated camera, for all advance ratios tested. These records are the closest representation of the flow encountered by the blade.

J = 0.56 is characterized by separation over almost the whole cycle. The separation starts at θ = 45° and the flow is normal to the blade at θ = 140°. There is a vortex forming on the upper surface which will travel aft and cause the turbulence on the return cycle. Naturally the torque required can be expected to be high and consequently the efficiency would be low.

As the advance ratio is increased, the flow becomes smoother until at $J = 4.50$, the velocity vector is parallel to the blade chord. Around $\theta = 180°$, the flow departs from the ideal condition due to the sudden blade pitch, but in this region the blade load does not give any thrust.

5.2 Blade Load Data Analysis

To gain a better insight of the propeller performance, blade loads were measured for all the advance ratios used in the flow analysis. The evaluation of the data poses the same difficulties experienced in the first test; the blade load records contain a vibratory variation of the load amplitude at a relatively high frequency.

An approximately sinusoidal thrust variation is to be expected over the period of one revolution. But superimposed on the load data there is a vibration which seems to have the natural frequency of the blade and its support. This can be seen when comparing the load records, Figure 31, and the static vibration of the blade, Figure 30 . The natural frequency of the blade is about 32 cps. Thus the presence of this vibration reduces the accuracy of the load analysis since the actual dynamic load effects and amplification of the natural frequency cannot be differentiated. In future tests, the use of a stiffer support for the blade could overcome this problem since semi - conductors have sufficient sensitivity to respond to a reduced strain.

The mean values of the oscillation were used for the load analysis. This makes the reduced blade load and thrust records smoother than they actually are, yet they still give good average values. Figure 30 shows the centrifugal and

inertia forces (model running in air) and the calibration curve used for data reduction.

Although the load records, Figure 31, show quite a variation over one cycle, the data had high repeatability. Several runs were made for the same advance ratio and the load traces were identical to each other.

Load peaks at $\theta = 160°$ and $\theta = 180°$ were caused by an intermittent bad electrical contact on one slip ring. The data at these two points has to be considered as unreliable.

Figure 32 shows the blade loads for $J = 0.56$ and $J = 3.50$, adjusted to compensate for the inertia and centrifugal blade forces. The forward cycle is well behaved, whereas the return cycle has considerable reduction of the loading, especially for $J = 3.50$. The reduction at the high advance ratio is caused by the following factors:

- the camber of the blades; since the blade operates on the return cycle at a negative angle of attack, the blade load due to camber reduces the contribution of the angle of attack load.
- the increased flow velocity causes an additional reduction in the angle of attack, as can be deduced from the vector diagram page 3 and blade flow parameters plotted in Figure 13.
- the turbulence, especially the one caused by the blade pitch at $\theta = 180°$, Figure 28.

The blade loads for $J = 0.56$, Figure 32, do not show the large reduction on the return cycle. At this advance ratio, the blade operates at such a high angle of attack that the increased inflow blade velocity does not have a great effect on the

flow parameter. The reduction in loading can be ascribed to the turbulent flow, Figure 26.

The blade load at $\theta = 0°$, at all advance ratios, is caused by the camber of the blade section and represents the load at zero angle of attack.

Overall, the trends of the load records agree reasonably well with the features observed in the flow.

5.3 Thrust Analysis

The thrust, namely the blade load component parallel to the forward motion, can be calculated from the loads measured normal to the blade. The general trends, Figure 33, are similar to the ones observed in the loads analysis.

The thrust of one blade is shown for $J = 0.56$ and $J = 3.50$, over a full cycle. In addition, the thrust of all four blades is summed using the appropriate phase shift and is shown on the same figure.

A considerable variation of the total thrust exists over one revolution. This is partially caused by the large reduction of the blade loads on the return cycle and the fact that only a small number of blades were used in the model. Upon increasing the number of blades to six or seven for a practical application, the thrust over a revolution would become smoother.

The mean thrust is used to calculate the thrust coefficient K_T at each advance ratio and the four available test points are shown in Figure 34. To show what could be expected with six blades, an estimate of K_T for a six bladed model is shown on the same figure. The efficiency could not be determined since the

instrumentation did not give torque readings.

It should be mentioned that the data presented contains two effects which must be taken into account if these results are used for a comparison with other test data. One is that the Reynolds Number is low ($R_n = 1.6 \times 10^4$). A more realistic Reynolds Number would give a higher blade load, especially in the region of high angle of attack. The other is the blade drag, which was not measured and which would contribute a reduction in the thrust.

Combining both effects, the net reduction on the reported thrust could be of the order of 5 to 8%. In any case, the results are only useful as a qualitative guide to correlate with the flow data. More instrumentation is required to measure the actual performance data.

6.0 BLADE LOAD CALCULATIONS

In the previous section, the blade load results were explained in terms of the observed flow. The next step will be to use the flow parameters developed in Section 5.1 to calculate the blade load for purposes of further comparison.

The method of calculation is based on a lifting line theory that was developed in Reference 4 and used in the previous study. Given the geometry and two-dimensional profile data, it is possible to derive a matrix of influence coefficients that relates the spanwise loading to a known spanwise distribution of incidence.

To simplify the calculation, the two-dimensional section data requires some approximation. A representative section with similar two-dimensional properties has to be selected. In the present case, the blade used in the test has a

camber of approximately 6% chord. The thickness/chord ratio varies from 5% at the tip to 25% at the root. Based on the above camber and thickness distribution, the closest available representation of the blade is given by NACA 65_2 - 415 . It is shown in Reference 3, page 131, that the lift curve slope is insensitive to variations in thickness. For the selected section, the slope is approximately 6.24/ radian. The angle of attack for zero lift (a_o) is about -3.10° .

Using the above data in conjunction with the basic planform data, shown in Figure 5, the spanwise loading distribution for unit angle of attack is:

x/L	0	.383	.707	.924
G_n/a	.4389	.4070	.3331	.1989

(G_n/a is defined in Reference 4)

The three dimensional lift curve slope and the spanwise center of pressure are derived from the load coefficients:

$$C_{L\alpha\ 3\text{-}D} = 4.07/\text{radian} \qquad \eta_{C.P.} = .436$$

The blade load can now be calculated for a given distribution of inflow parameters. This is done for J = 3.50 only, since at the other advance ratios the blade stalls in some regions and the calculation would not give realistic values. Using the angle of attack and velocity distributions from Figure 13, the blade load is calculated at 15° intervals by the formula:

$$\text{Blade Load} = \text{Lift} = \frac{\rho}{2} \nabla^2 C_{L_{\alpha\ 3\text{-}D}}\, a\, A$$

The results of this calculation are shown in Figure 35 as a comparison to the measured blade load and thrust from Figures 32 and 33 .

On the forward cycle, the calculation and measurements agree favorably, but on the return cycle some larger deviations exist. In the region from $\theta = 190°$ to $\theta = 260°$ the calculated blade load is much higher. This is mainly caused by the turbulent flow existing in this region (Figure 28) which cannot be considered in the calculation. For the most part the calculated blade load and thrust follows reasonably close to the measured pattern.

7.0 COMPARISON OF TEST RESULTS WITH P/D = .70π DATA

An earlier test program using similar techniques (for a propeller of P/D = .70π) is reported in Reference 1 . Since similar techniques are used some of the test data are compared, although the test conditions were not identical. For example, for P/D = .70π, the maximum efficiency is attained at J = 1.75, whereas in the case of P/D = π/.70 it is attained at J = 3.50 .

At low advance ratios, the general flow pictures for the high pitch ratio propeller show a greater disturbance from the ideal inflow conditions, because of the higher angle of attack; Figure 14 in this report and Figure 7, Reference 1 .

This effect is reversed at the advance ratio with maximum efficiency, where in the case of the high pitch ratio propeller, the disturbance was less, due to the high free stream velocity; Figure 16 in this report and Figure 9, Reference 1.

Further details can be seen in the sequences using the articulated camera, by comparing the present Figure 26 with Figure 17 in Reference 1, both cases

being at a low advance ratio. Each flow pattern contains a strong disturbance of the flow, due to the high angle of incidence; the disturbance is stronger in the present propeller. The stall in Figure 27 on the forward region occurs early and causes strong turbulent effects on the return cycle.

The articulated sequences at the maximum efficiency advance rates are shown in Figures 28 for $\pi/.70$ and Figure 20, Reference 1. Because of the higher inflow velocity, there is much less curvature present in the high pitch ratio flow. In the region of $\theta = 180°$, both cases show the vortex due to the blade pitch. The vortex has less influence on the high pitch ratio due to the high free stream velocity, but still causes a considerable disturbance in the flow.

The blade load records for both tests show the high frequency vibration on the load amplitude. The frequency for the high pitch ratio test, Figure 30, is somewhat higher than the low pitch ratio test. The blade is smaller and lighter than the blade used in the earlier test and therefore has a higher natural frequency. This observation confirms the earlier suggestion that this vibrationary load variation is caused by the natural frequency of the blade.

The blade used for the higher pitch ratio test was rectangular, whereas the .70πtest blade had a taper of 0.53 . This could explain why the angle of attack varied considerably over the span in the earlier test, whereas the data presented in this report is more uniform, within the usual scatter.

In both test programs the flow visualization gives a good insight of flow details. These details should help to formulate better assumptions for mathematical models used in the analysis of vertical axis propellers.

8.0 CONCLUSIONS

The program is an extension of an earlier test to study the cycloidal propeller by flow visualization. The results presented contain a large amount of information which can be summarized as follows:

1) The efficiency of a high pitch ratio propeller at low advance ratio is low due to early blade stalls, which cause a high drag and torque.

2) At the advance ratio with maximum efficiency, the free stream velocity is increased by 10 to 12% on the return cycle, causing a reduction in angle of attack.

3) Cambered blade sections are not recommended for future high pitch ratio designs, since the blade load is reduced on the return cycle by the cambered effect.

4) The results presented can be used as a guide to develop modified cycloidal blade motion, which would generate more thrust.

5) The strong variation of angle of attack along the span reported in the .70π test could not be observed. It appears that the uniform angle of incidence in this test is related to the rectangular blade form used for the blade.

6) The flow visualization pictures and measured blade loads can be used to develop appropriate theoretical models for analysis.

To enhance the value of flow visualization tests, the following steps should be pursued:

1) Operate the existing model at high rpm to increase the Reynolds Numbers.

2) Develop the articulated camera technique to determine the inflow parameters accurately from articulated sequences.

3) Perform flow visualization tests with a model on which the pitch ratio can be varied to test a wider range of operating conditions. This would require the design and construction of a new model.

With the above modifications, detailed studies could be carried out using:

1) Different blade planforms and blade sections.

2) Modified cycloidal propellers using the experience gained from earlier tests.

3) Study the flow with the control center offset.

9.0 REFERENCES

1) McKillop, J. A., "A Study of Flow Through a Vertical Axis Propeller" ERA Report 60/1, April 1965.

2) Ficken, N. L., "Conditions for the Maximum Efficiency of Cycloidal Propellers" Paper presented to SNAME, Chesapeake Section, April 1966.

3) Abbot, I. H. and von Doenhoff, A. E., "Theory of Wing Sections" Dover Publications, Inc., 1959.

4) De Young, J. and Harper, C. W., "Theoretical Symmetric Span Loading at Subsonic Speeds for Wings Having Arbitrary Plan Form" NACA Report 921, 1948.

Figure 1 - Schematic Geometry of Cycloidal Propeller and Blade Angle

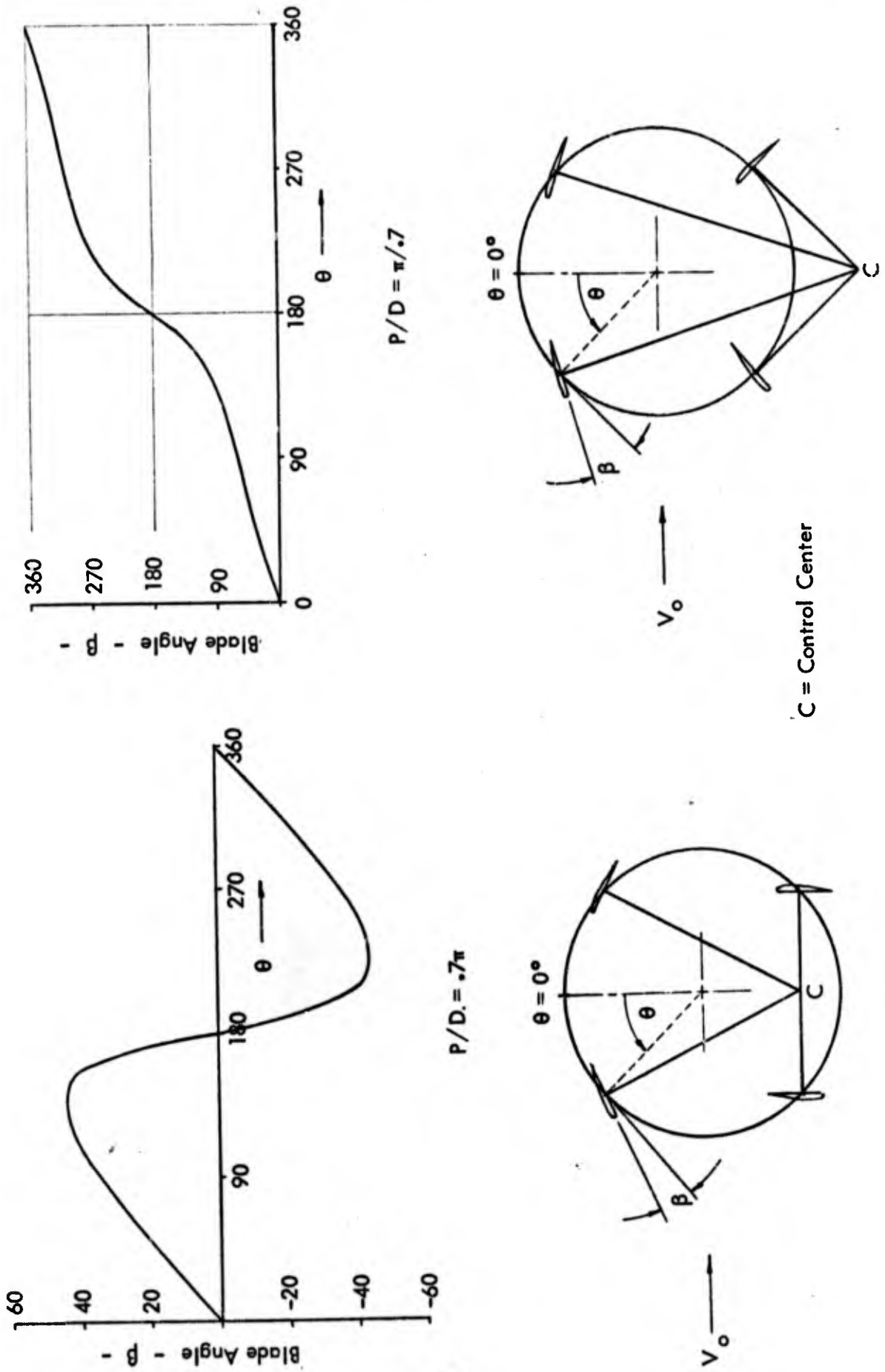

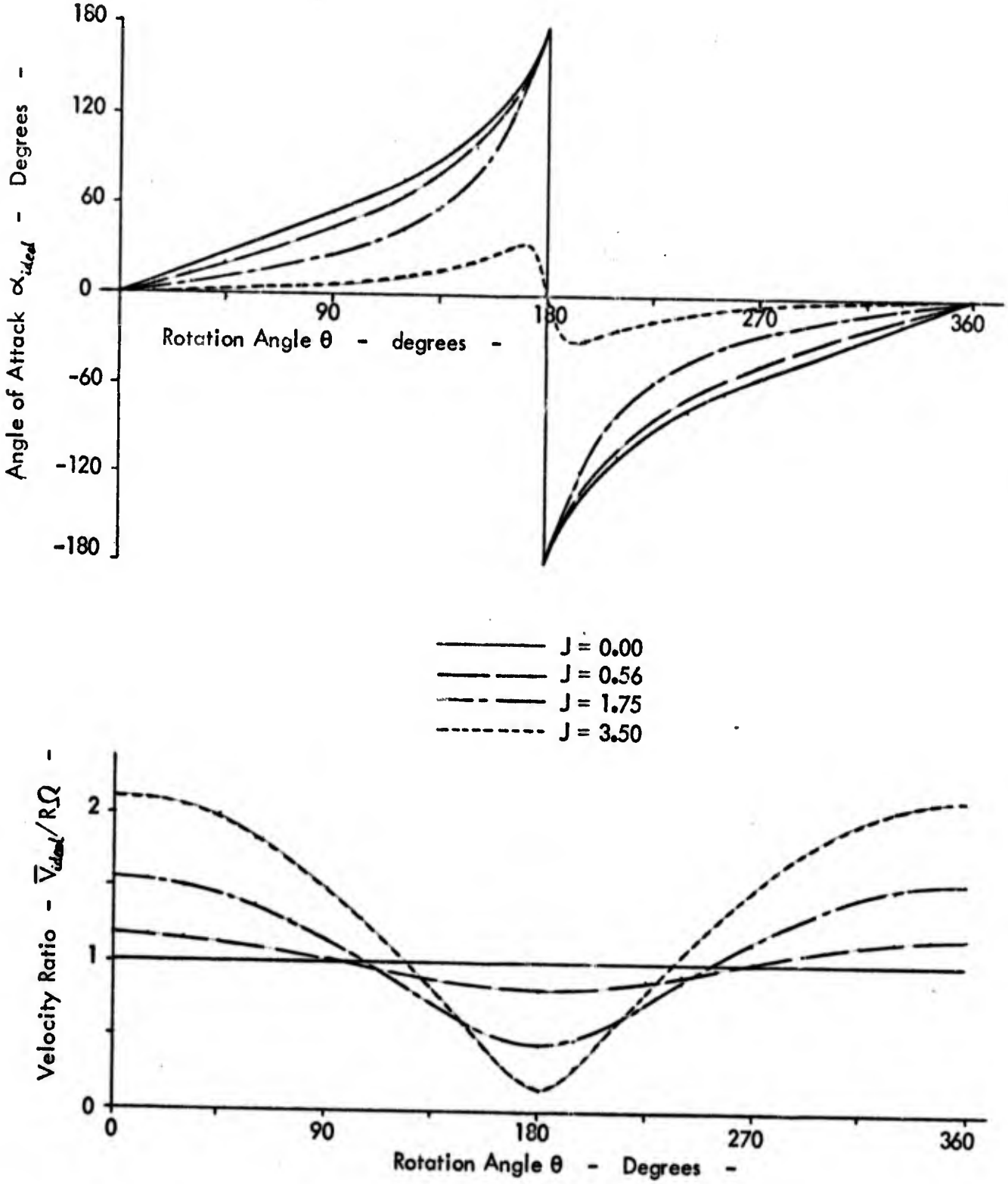

Figure 2 - Ideal Flow Parameters - P/D = π/.70

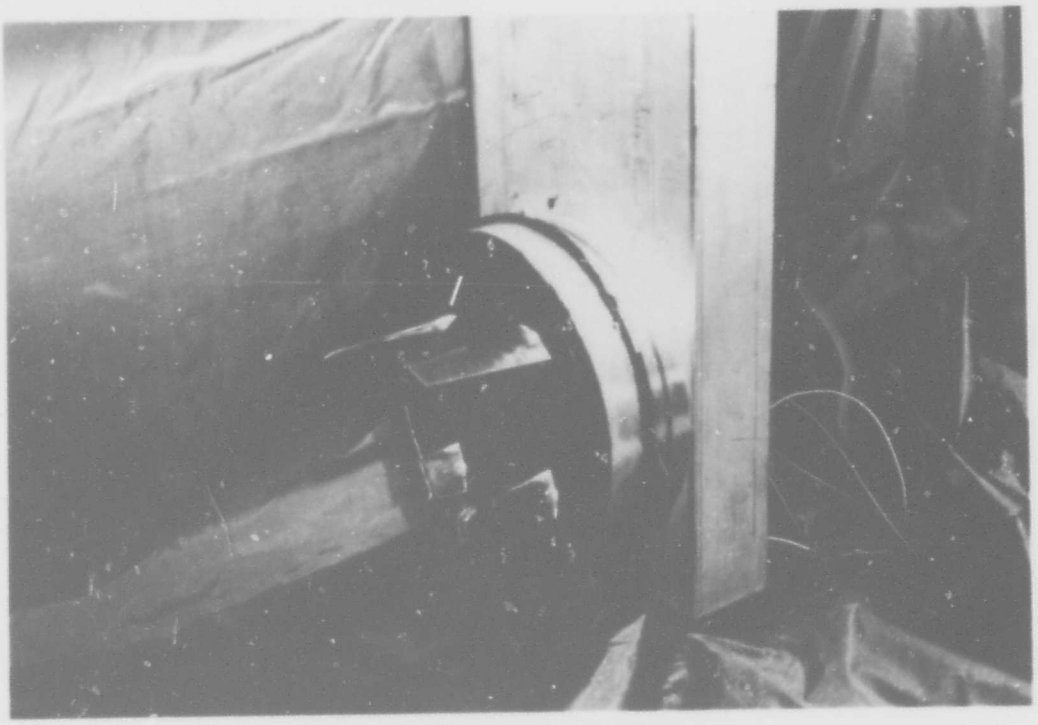

Figure 3 - Propeller Assembly

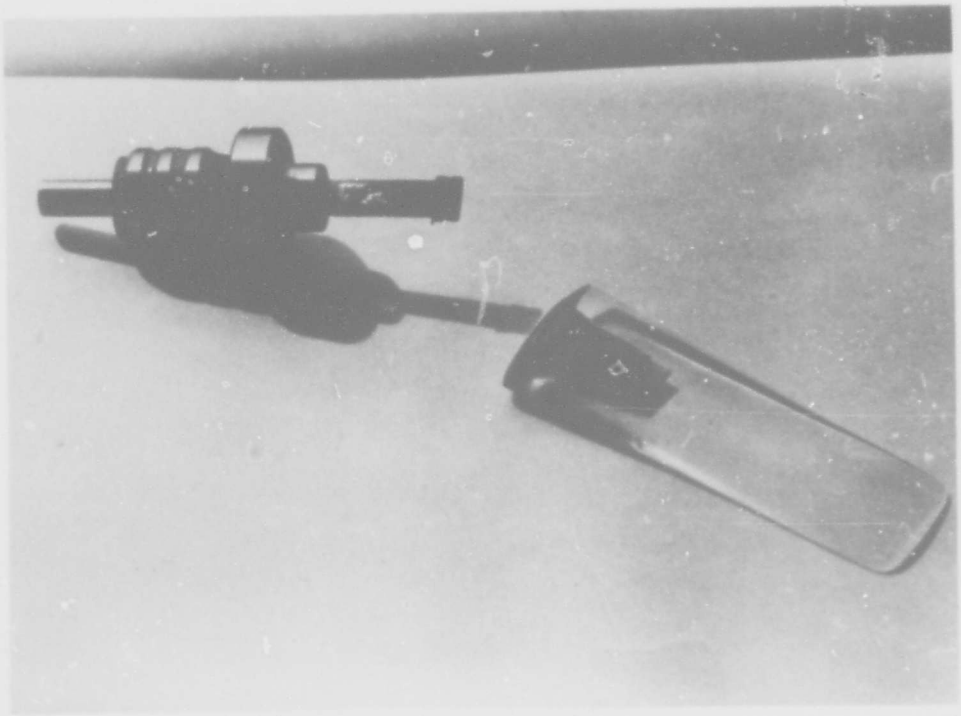

Figure 4 - Blade and Straingage Assembly

Length	- 3.15 in.	L/D	- 0.50
Average Chord	- 1.11 in.	Aspect Ratio	- 5.70
Blade Area	- 3.50 in.^{2}	Blade Area Ratio	- 0.71 (4 Blades)

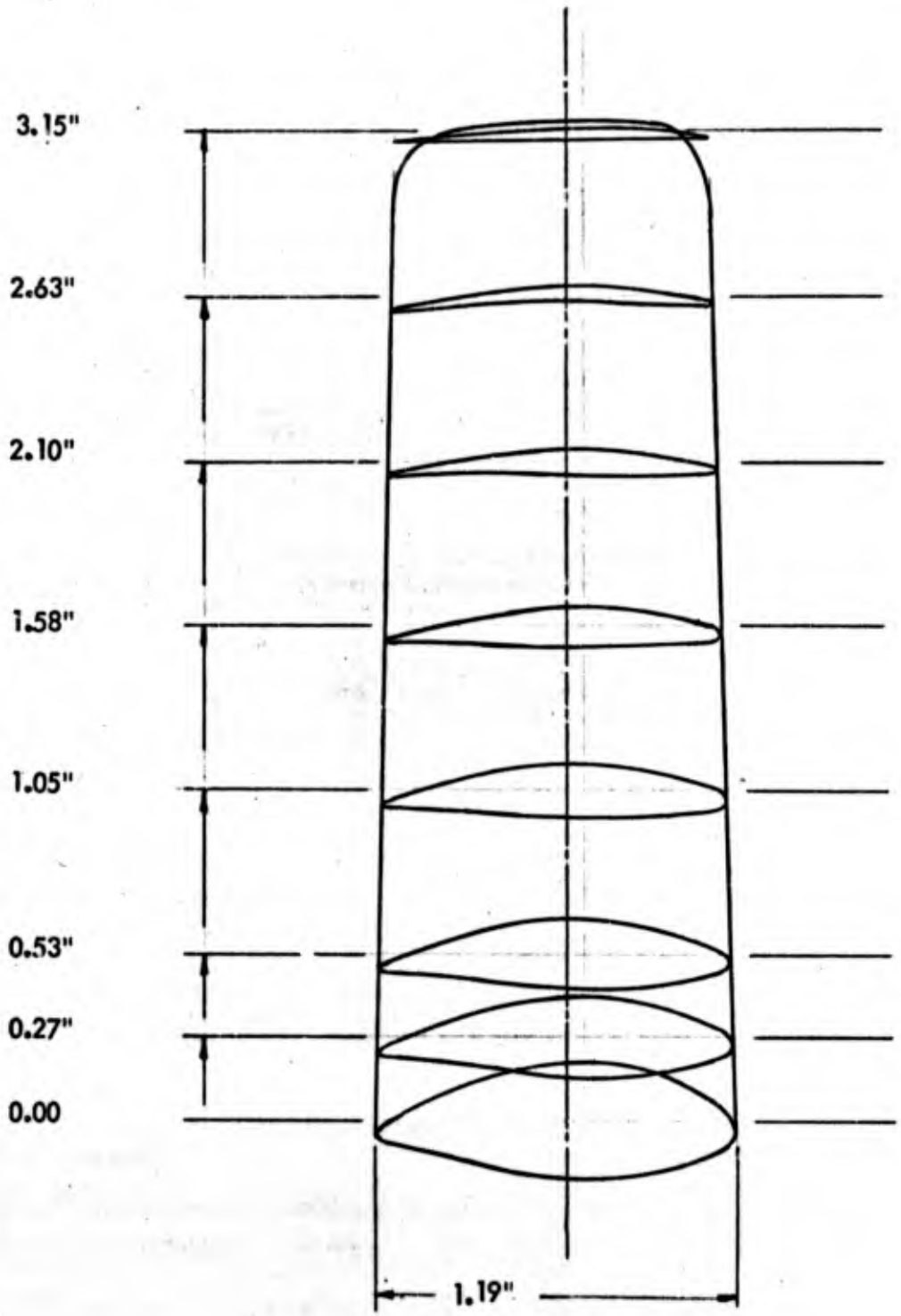

Figure 5 - Blade Planform Used for Test

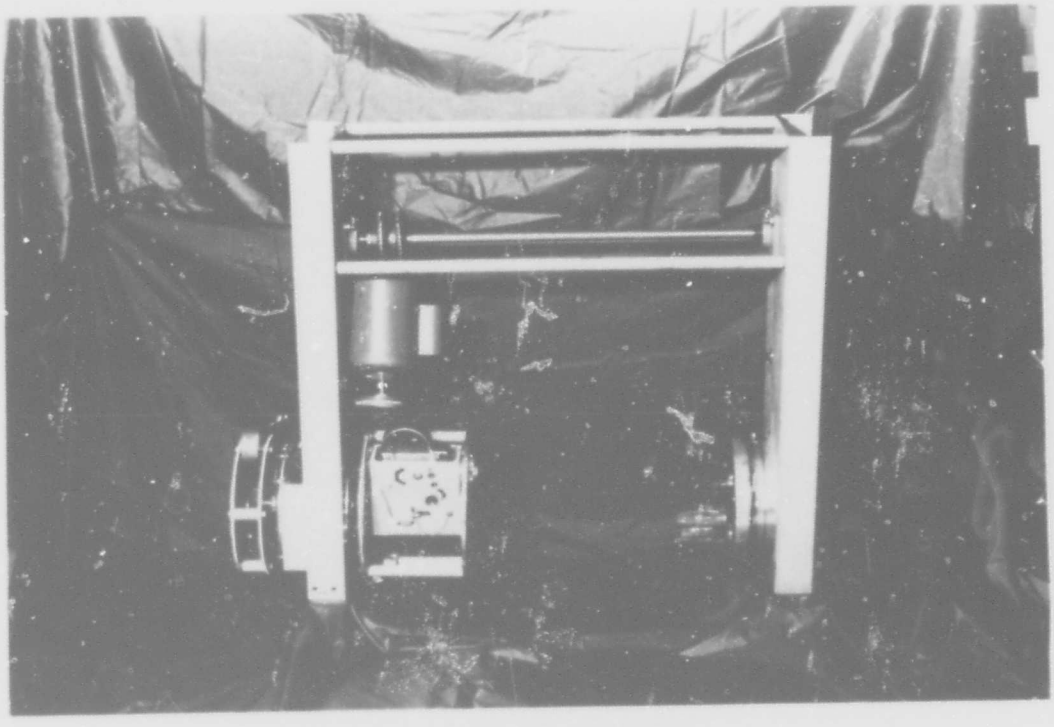

Figure 6 - Assembled Test Model

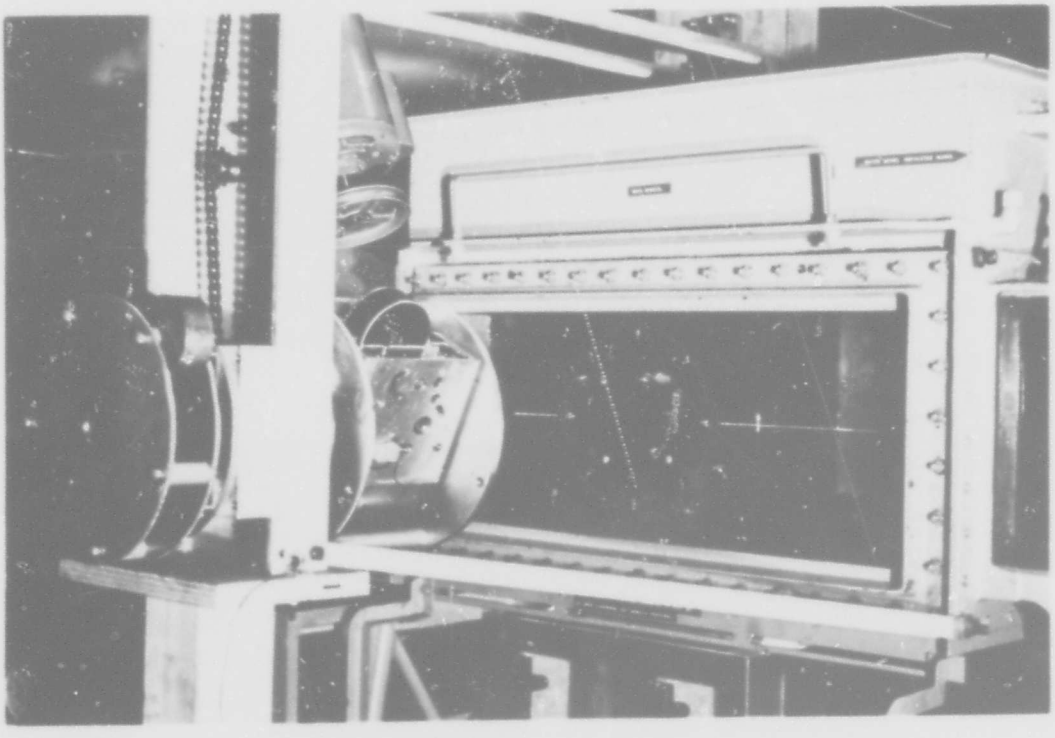

Figure 7 - General View of Water Tunnel with Model Installed

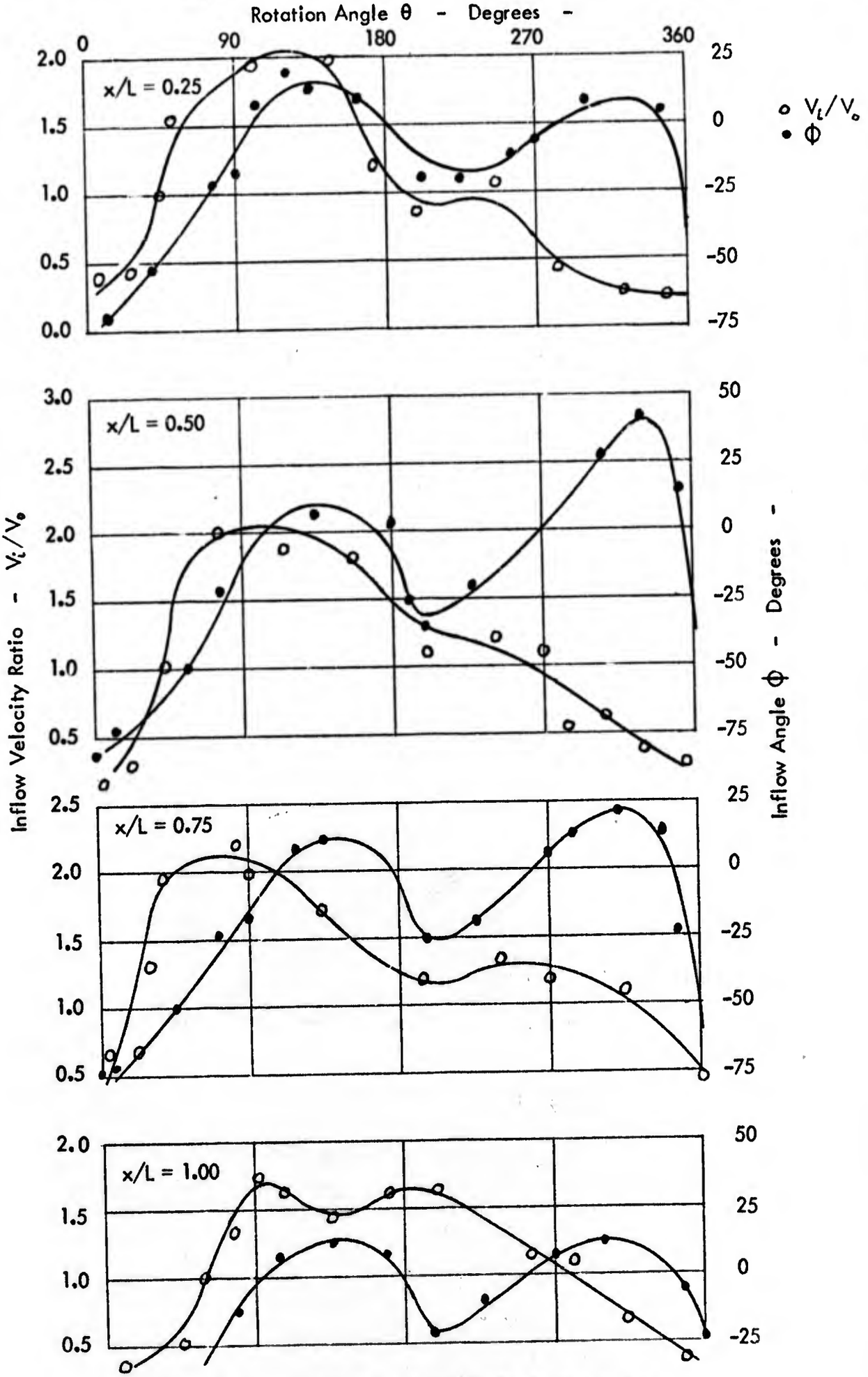

Figure 8 - Measured Inflow Properties at J = 0.56

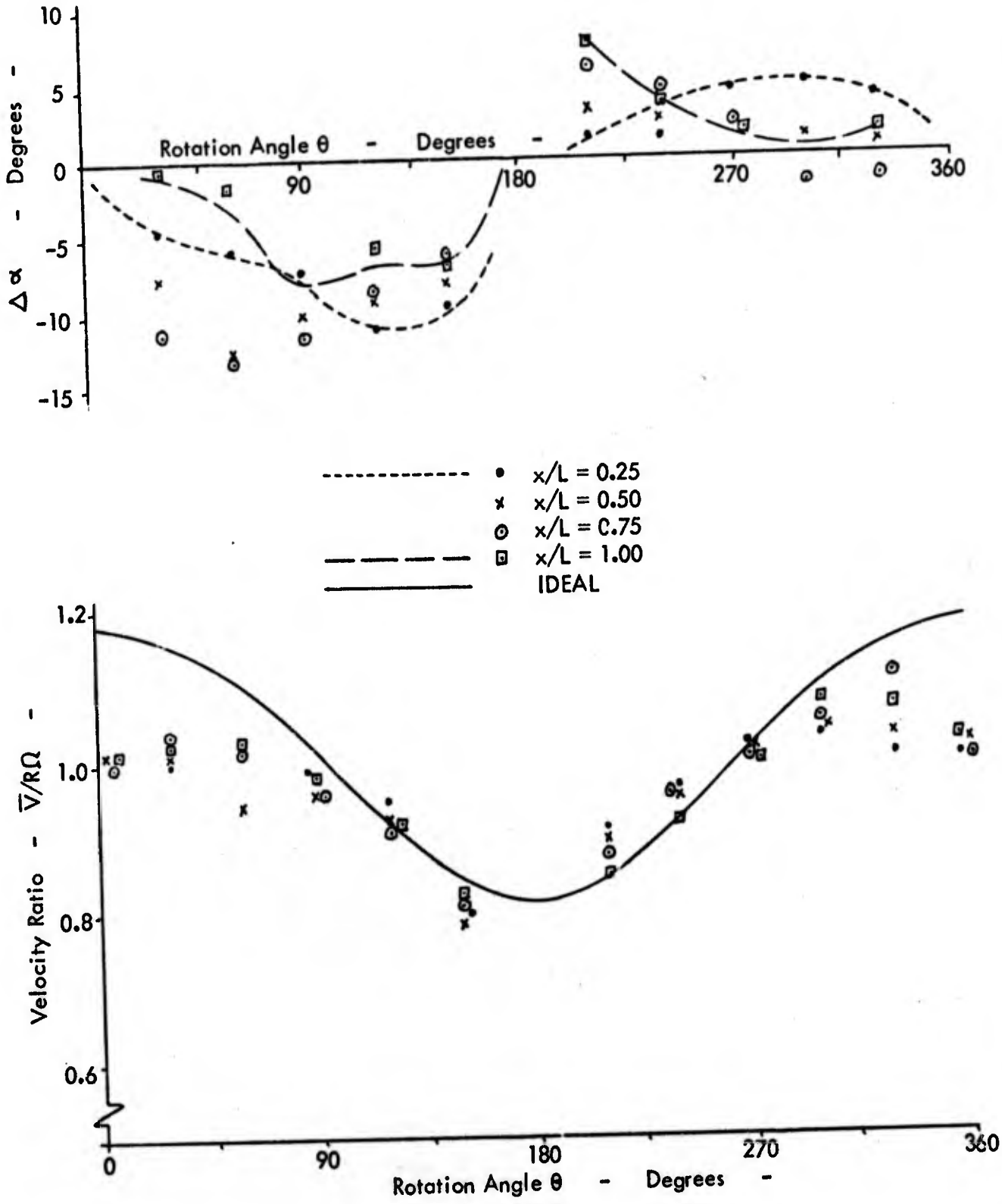

Figure 9 - Blade Flow Parameters - J = 0.56

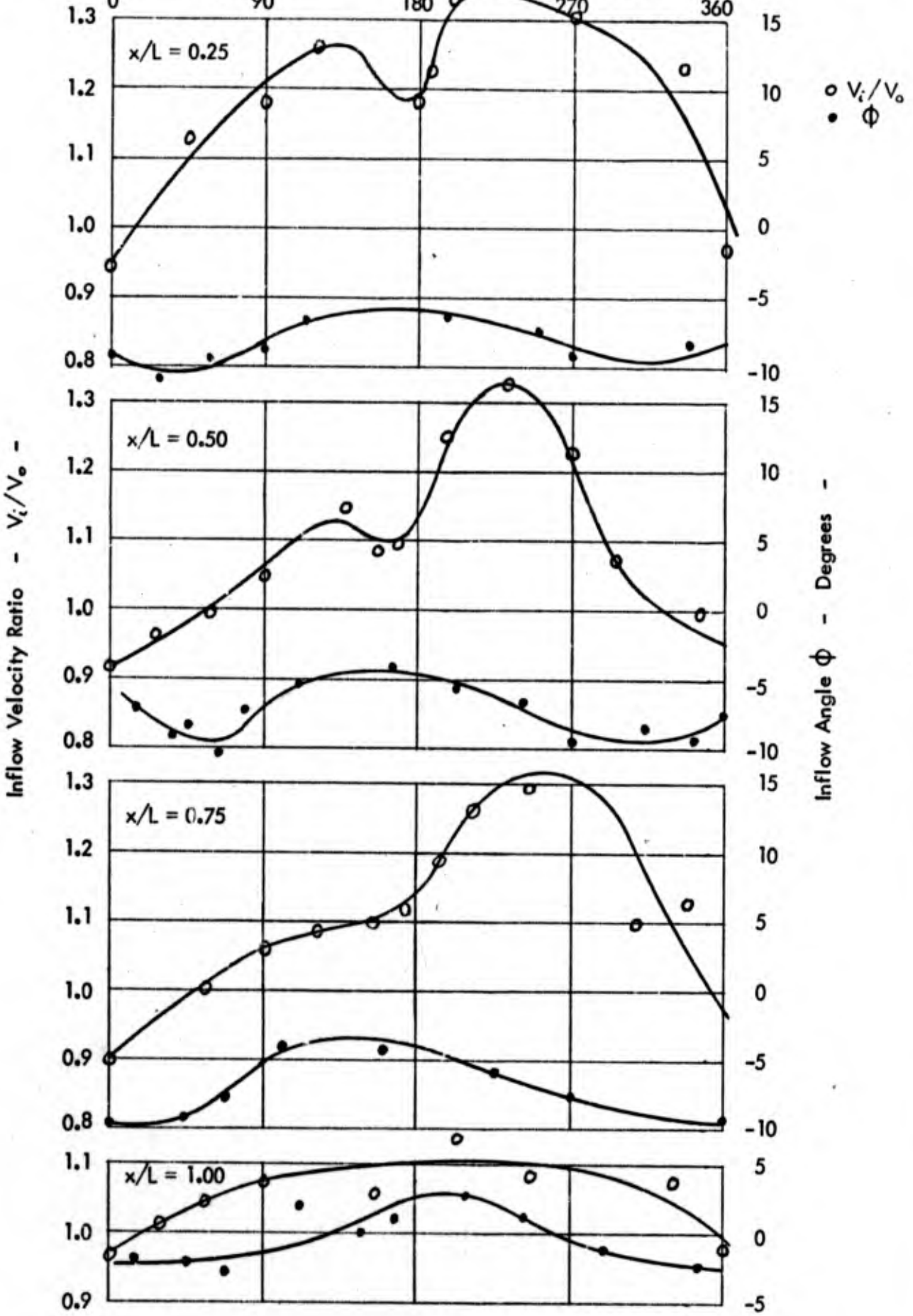

Figure 10 - Measured Inflow Properties at J = 1.75

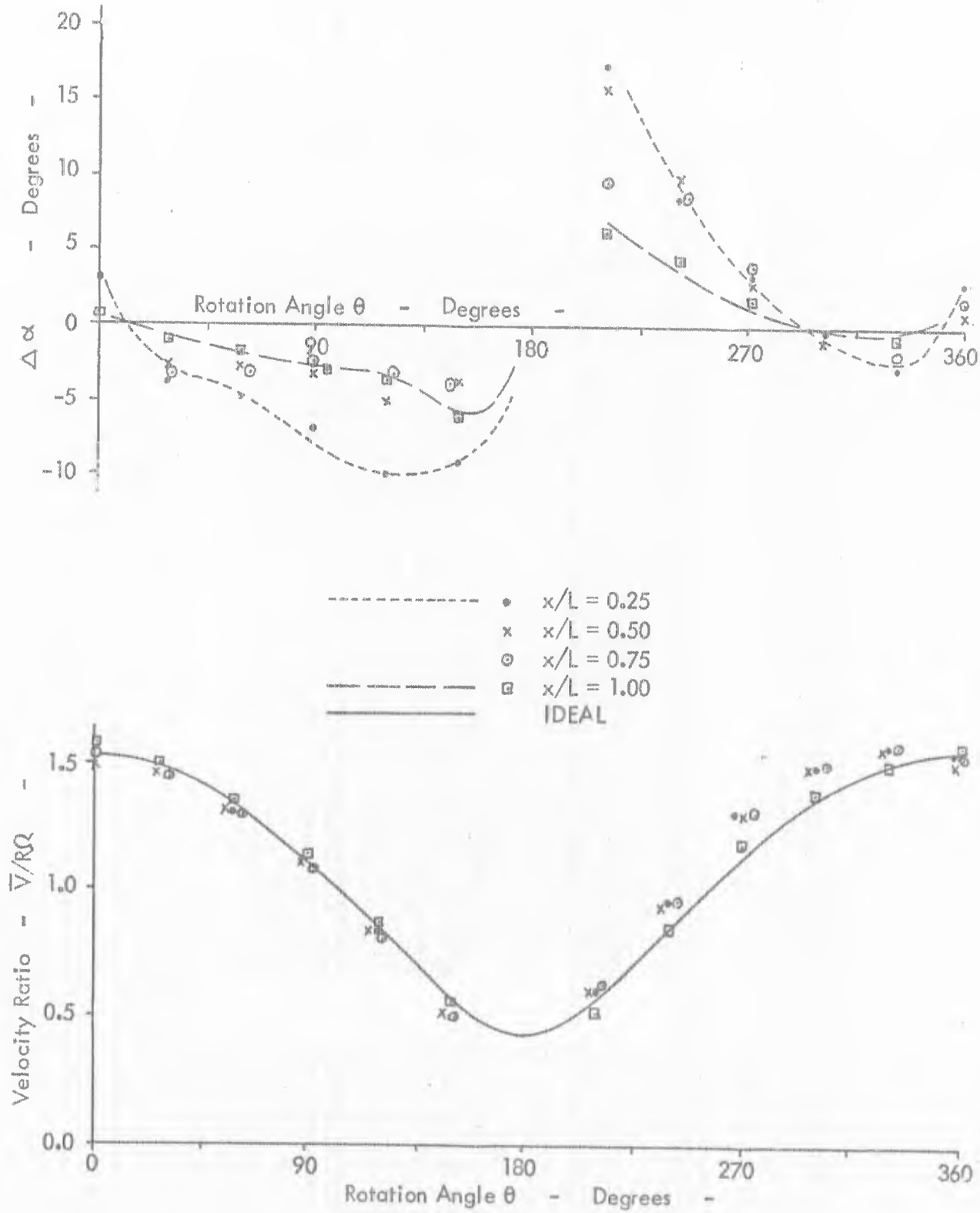

Figure 11 - Blade Flow Parameters - J = 1.75

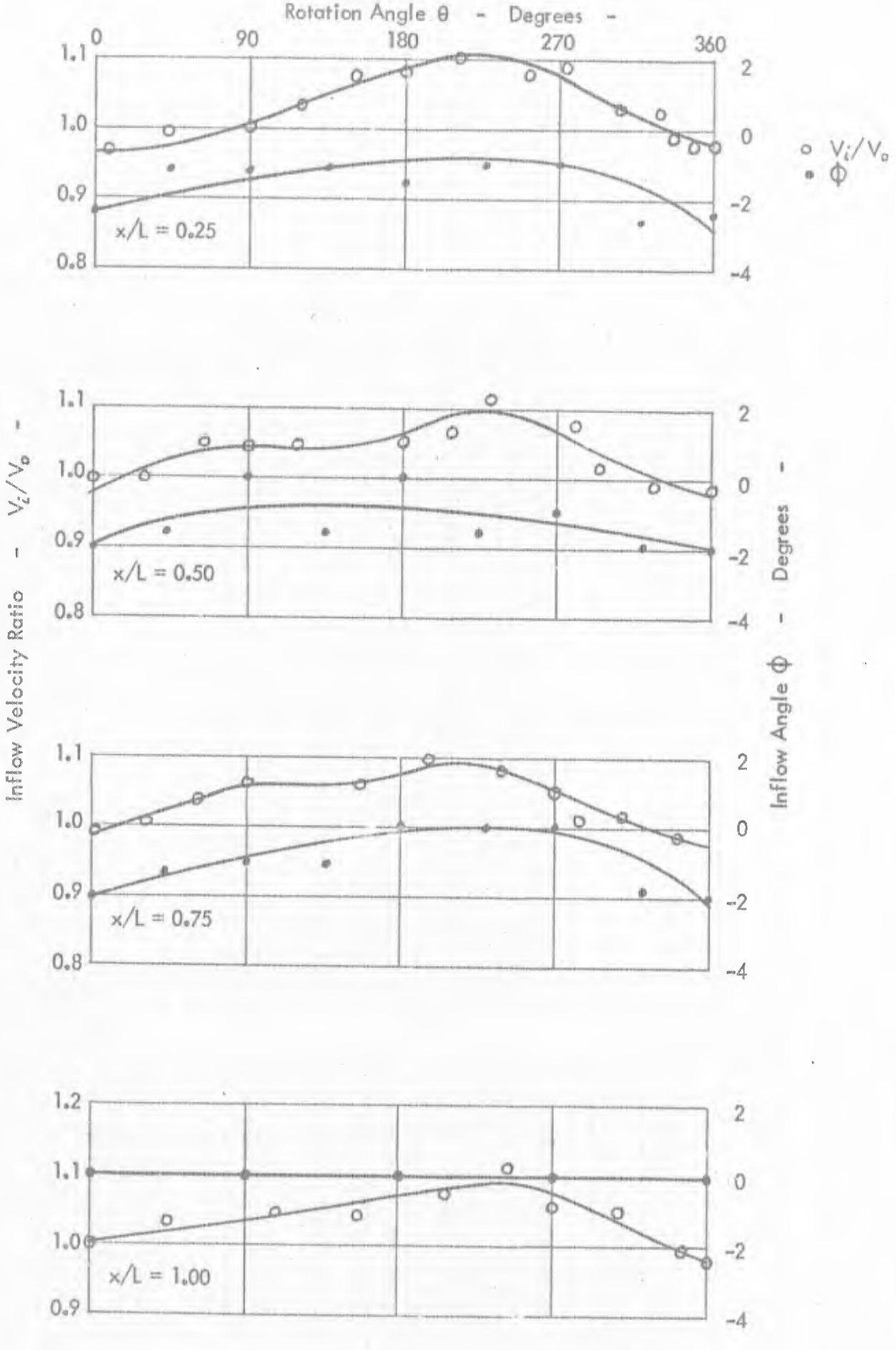

Figure 12 - Measured Inflow Properties at J = 3.50

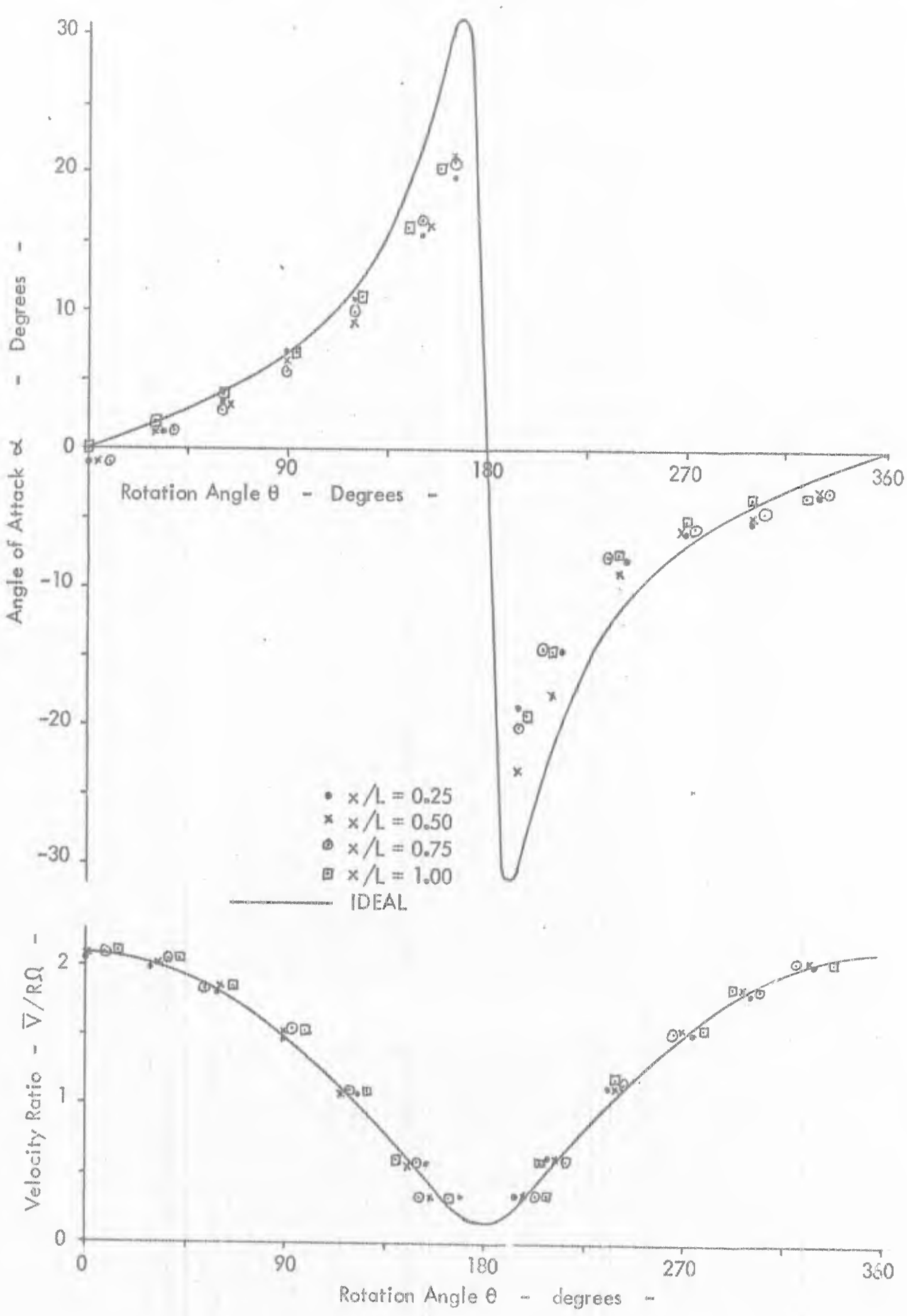

Figure 13 - Blade Flow Parameters - J = 3.50

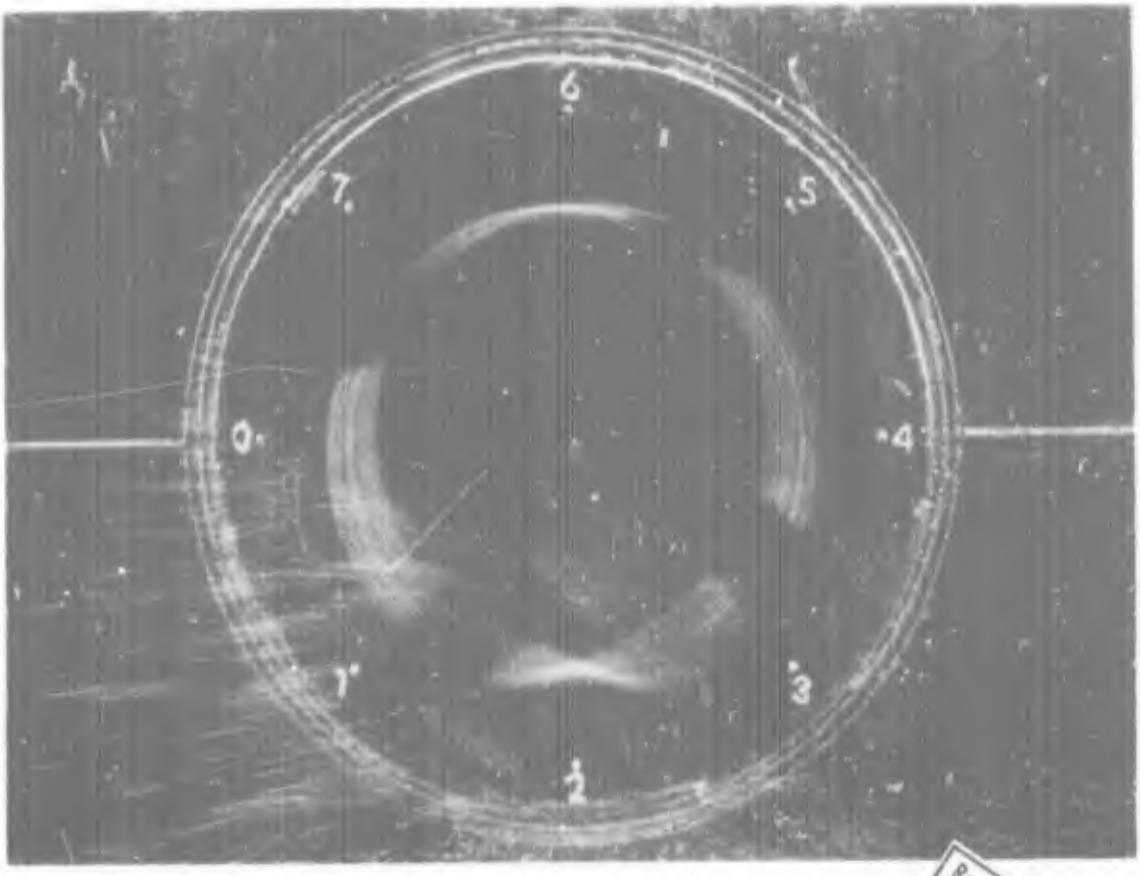

Figure 14 - General Flow Section - J=0.56 - x/L=0.5

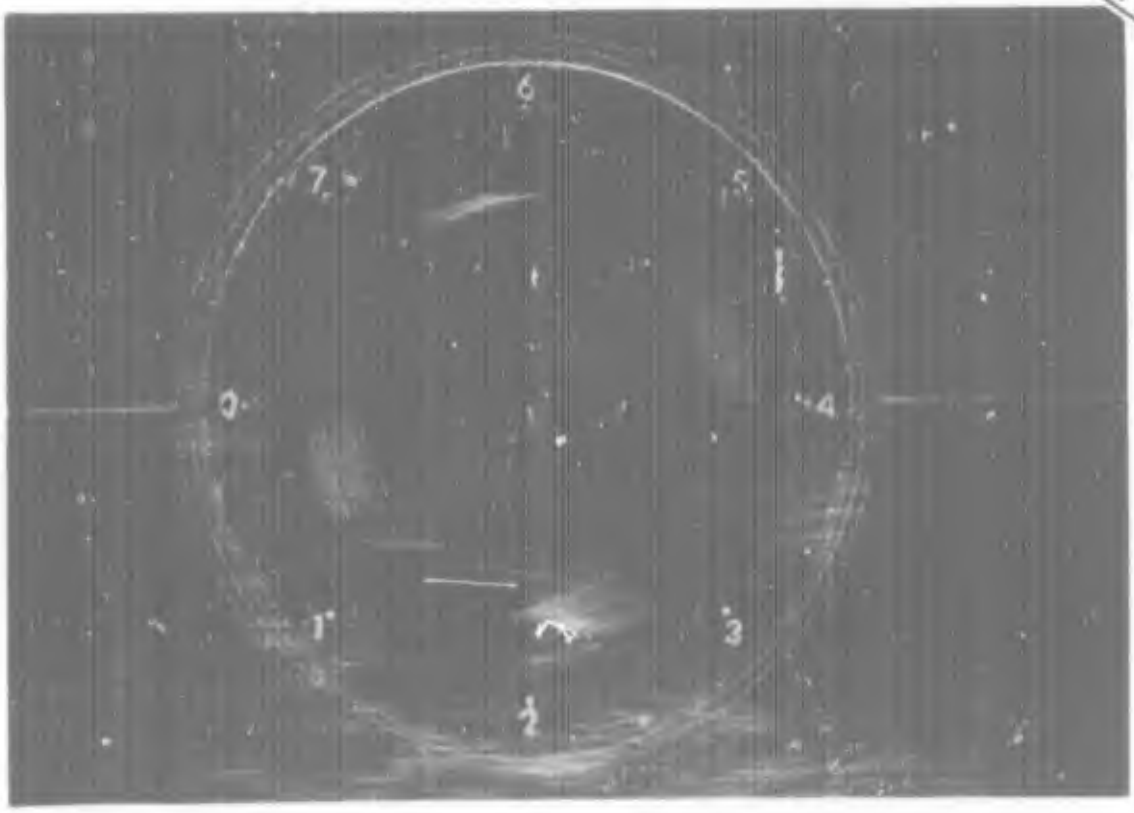

Figure 15 - General Flow Section - J=1.75 - x/L=0.5

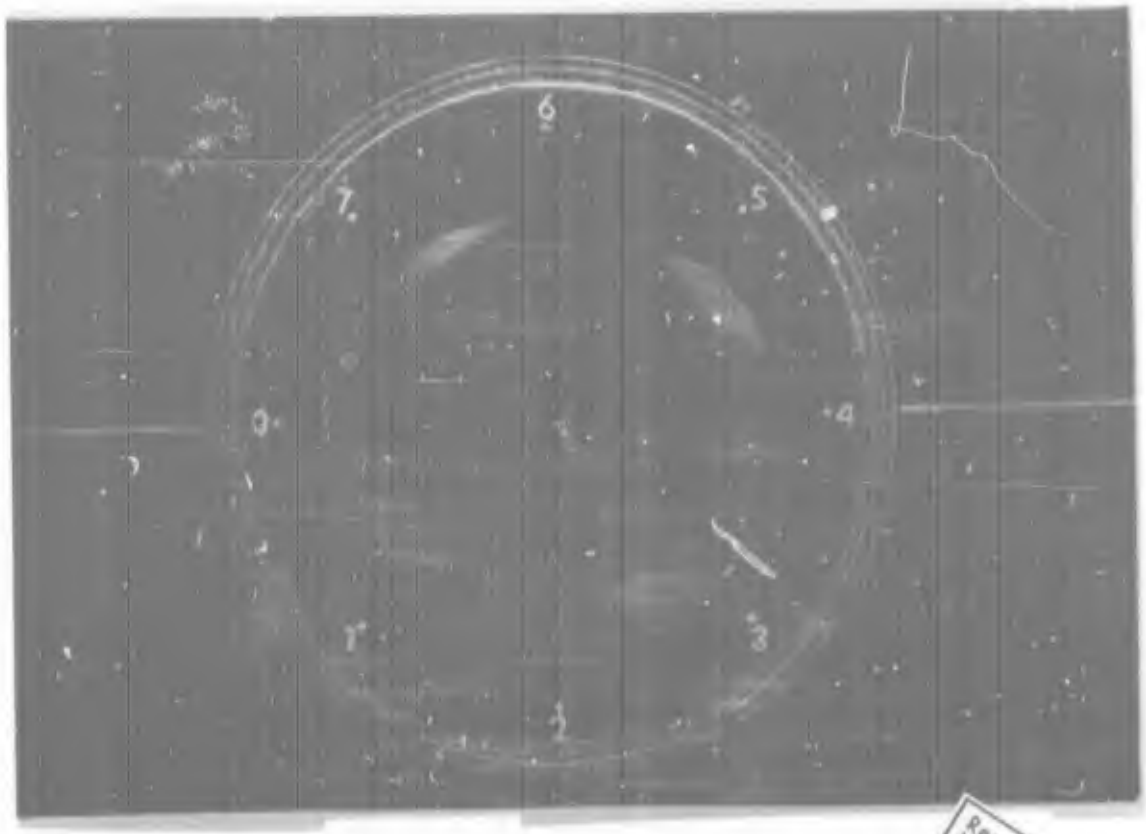

Figure 16 - General Flow Section - J=3.50 - x/L=0.5

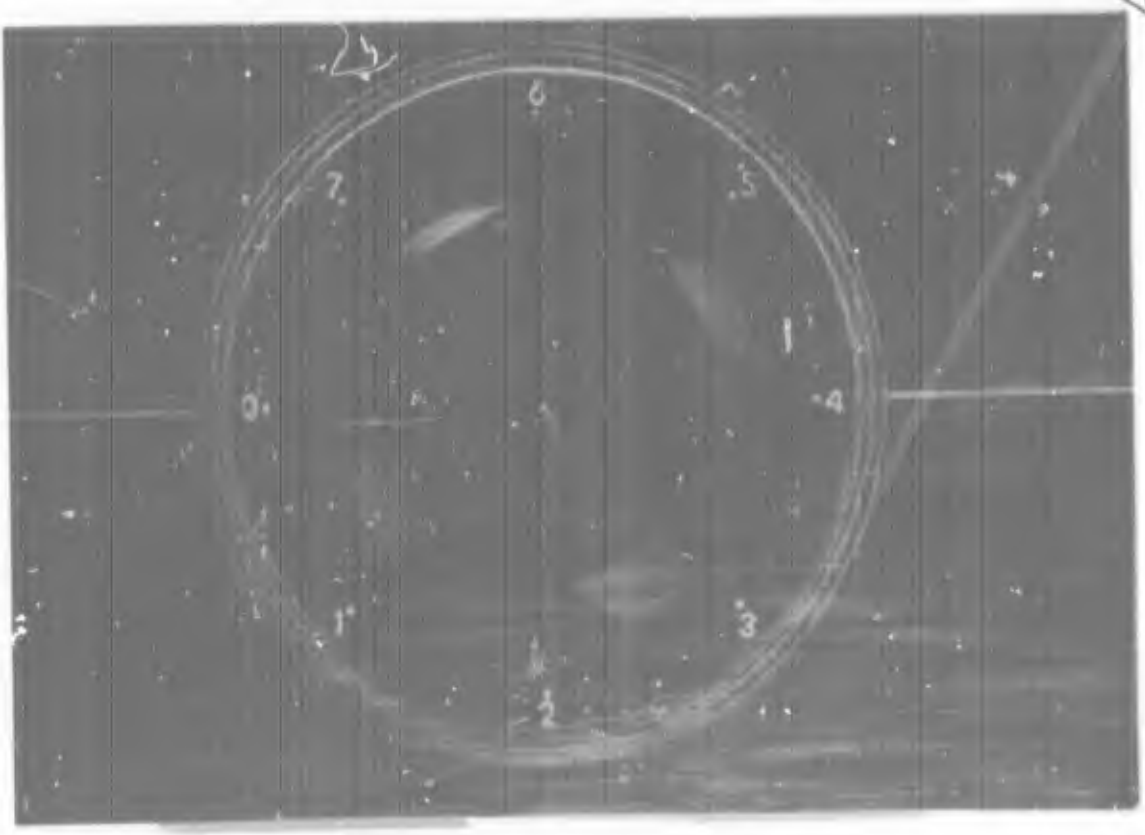

Figure 17 - General Flow Section - J=4.50 - x/L=0.5

Figure 18 - Transverse Section at Center Line - J=.56

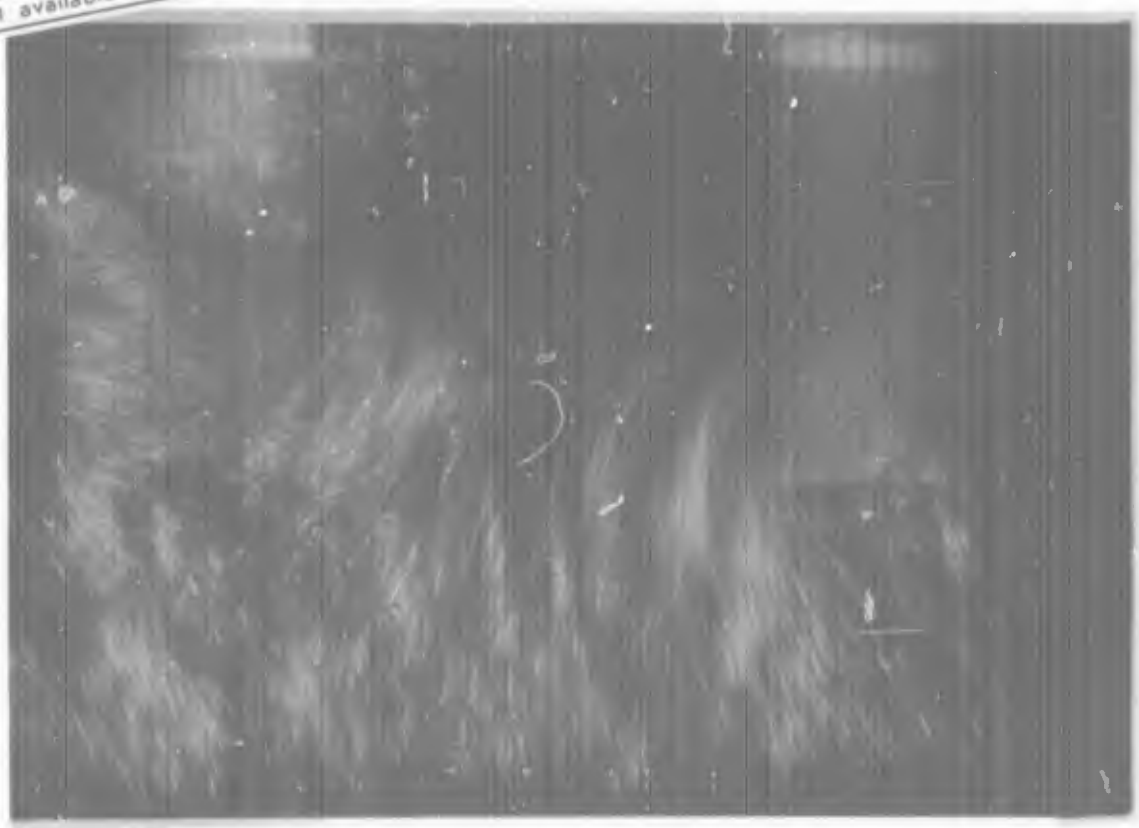

Figure 19 - Transverse Section at Rear Radius - J=.56

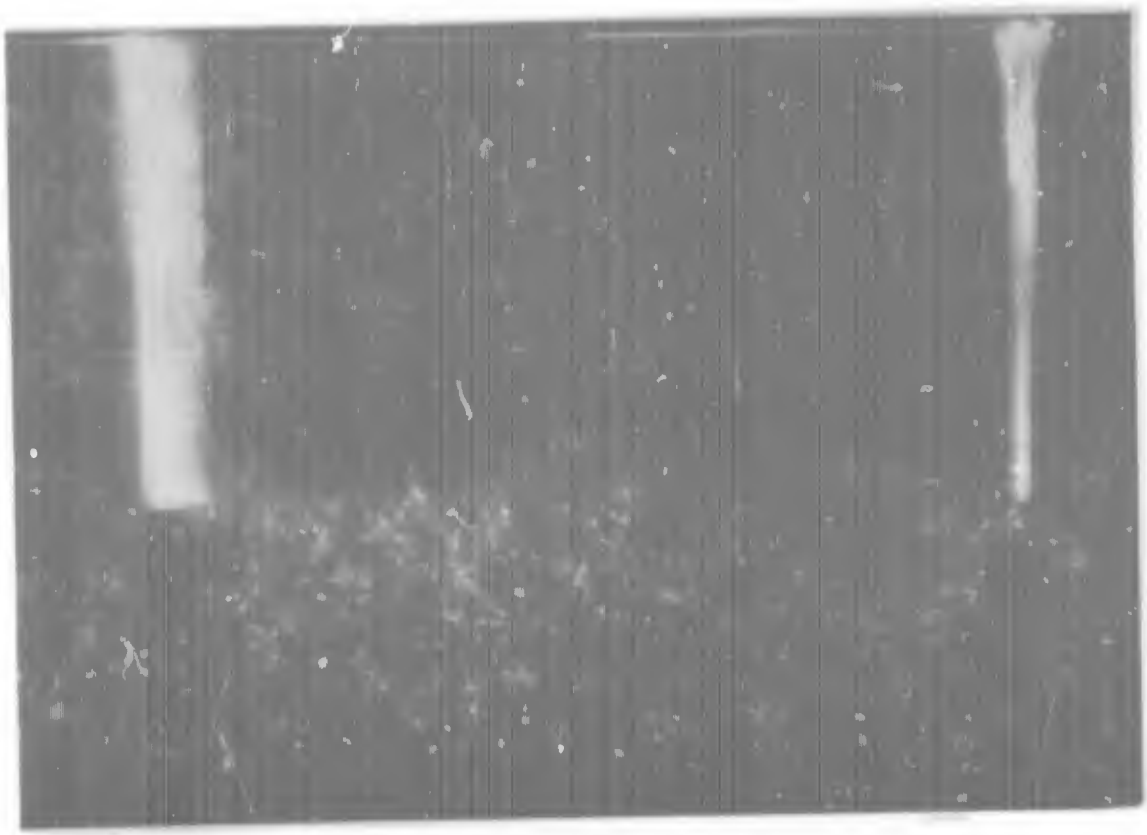

Figure 20 - Transverse Section at Center Line - J=3.50

Figure 21 - Transverse Section at Rear Radius - J=3.50

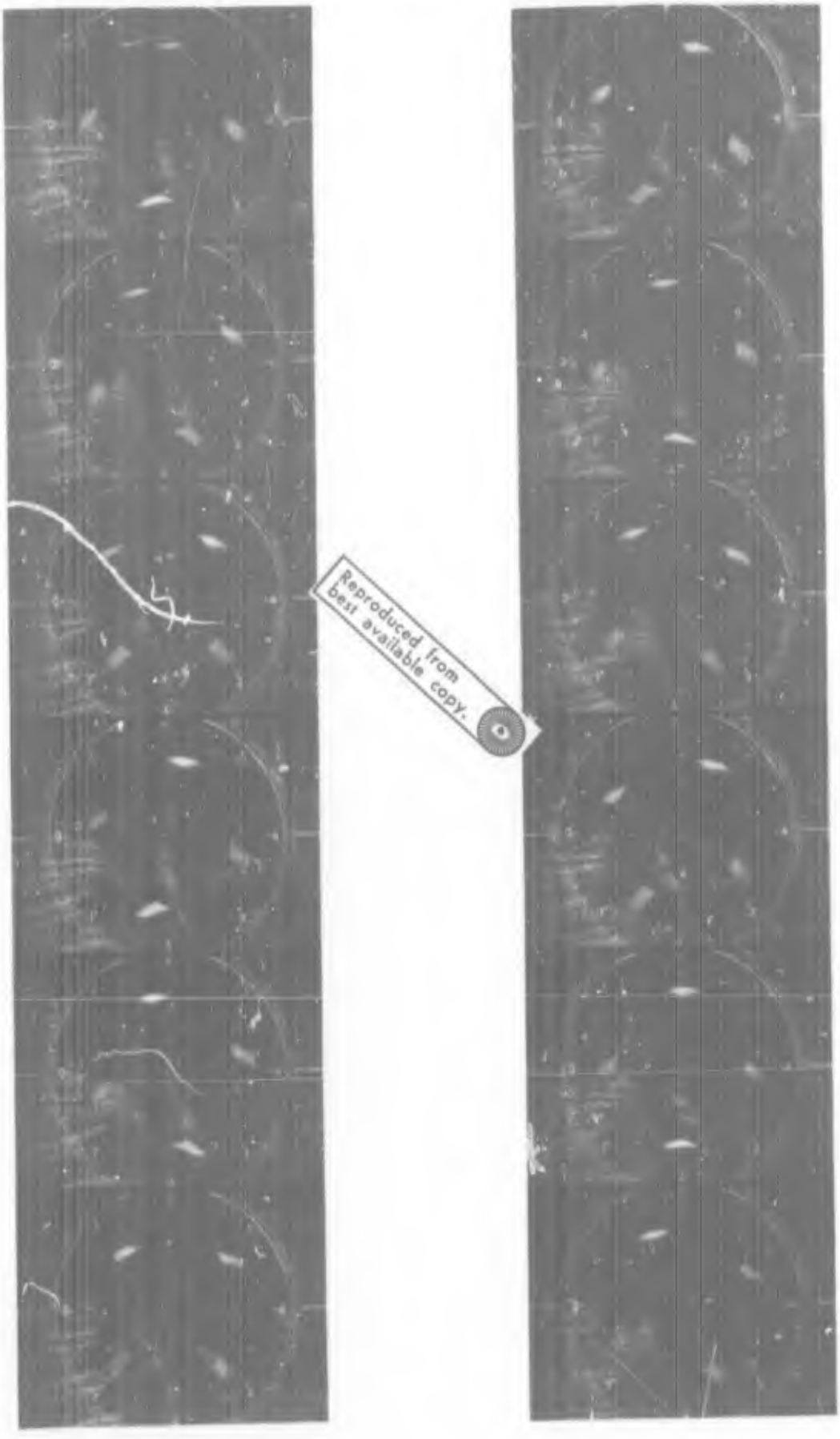

Figure 22 - One Revolution - J=0.56 - x/L=.50

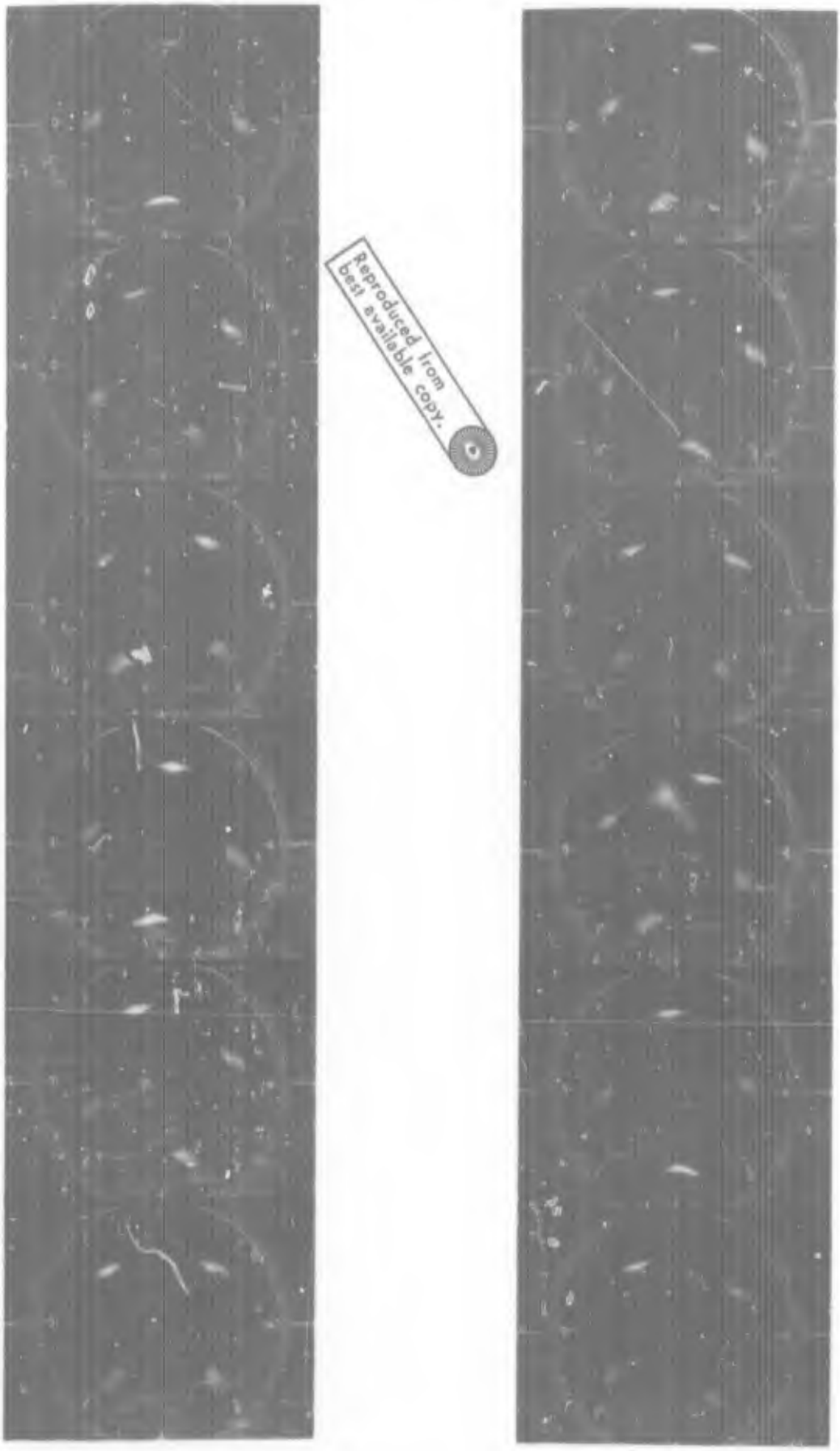

Figure 23 - One Revolution - J=3.50 - x/L=0.50

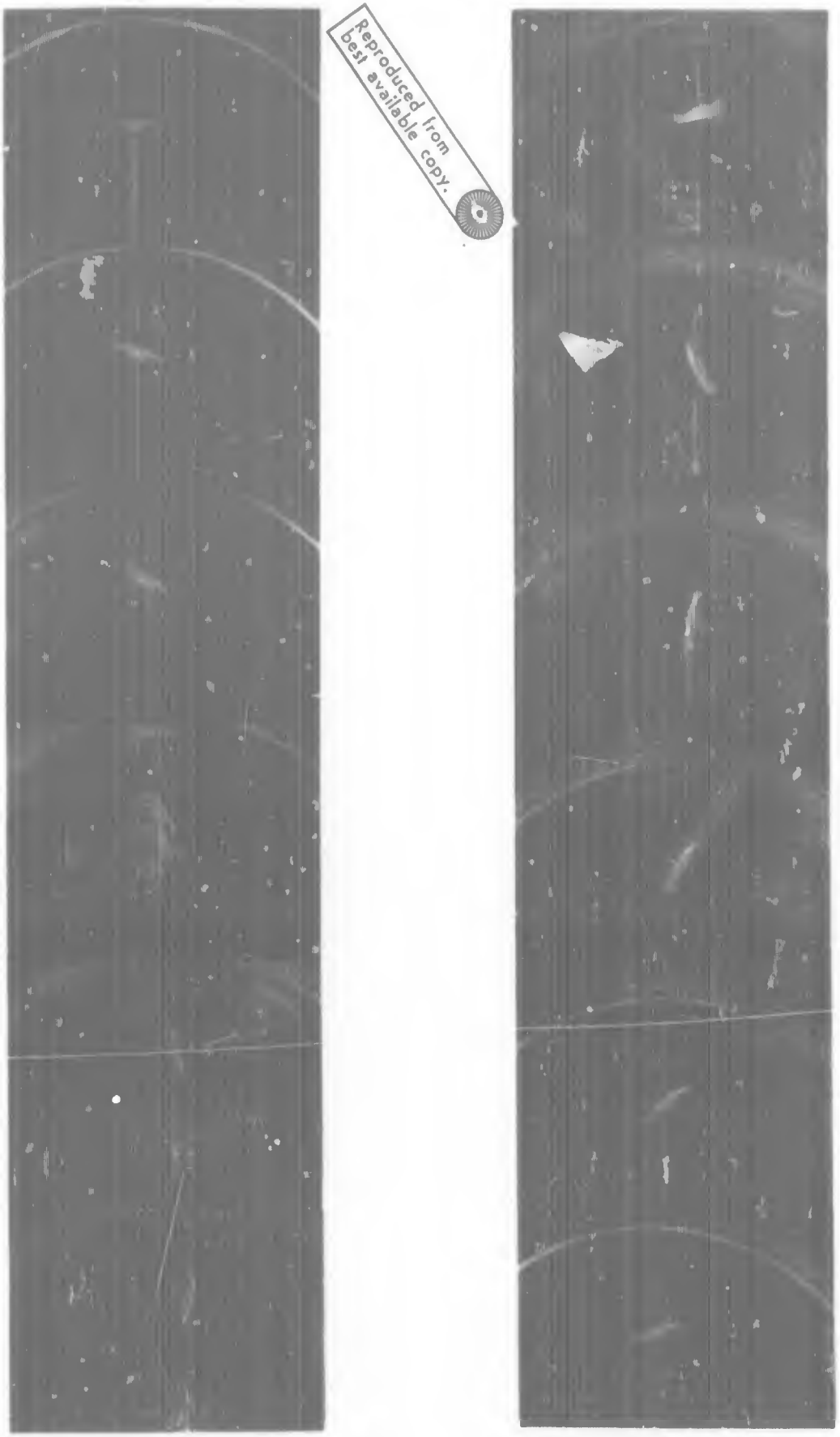

Figure 24 - One Cycle - J=.56 - x/L=0.5 Rotating Camera

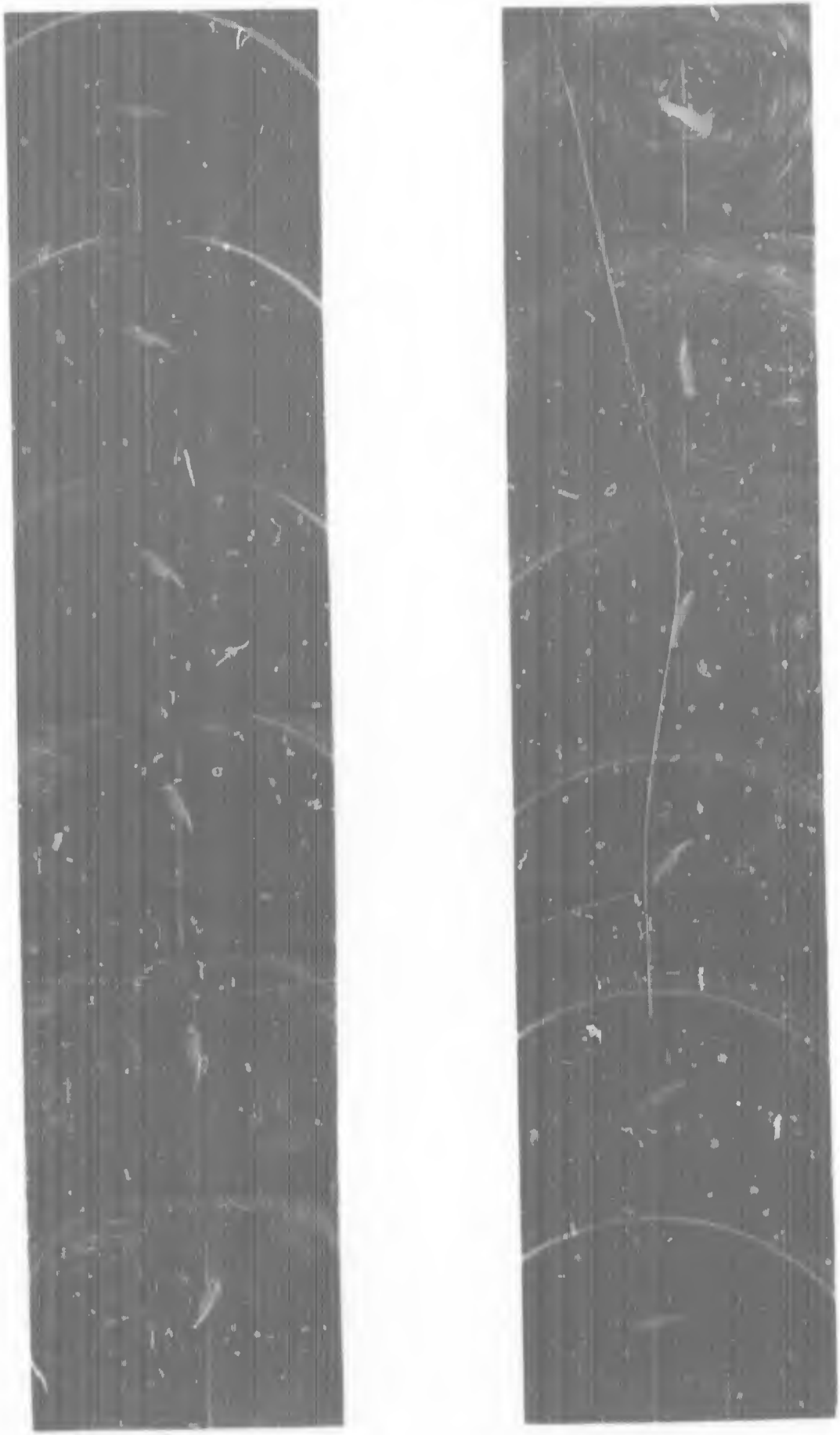

Figure 25 - One Cycle - J=3.50 - x/L=0.5 Rotating Camera

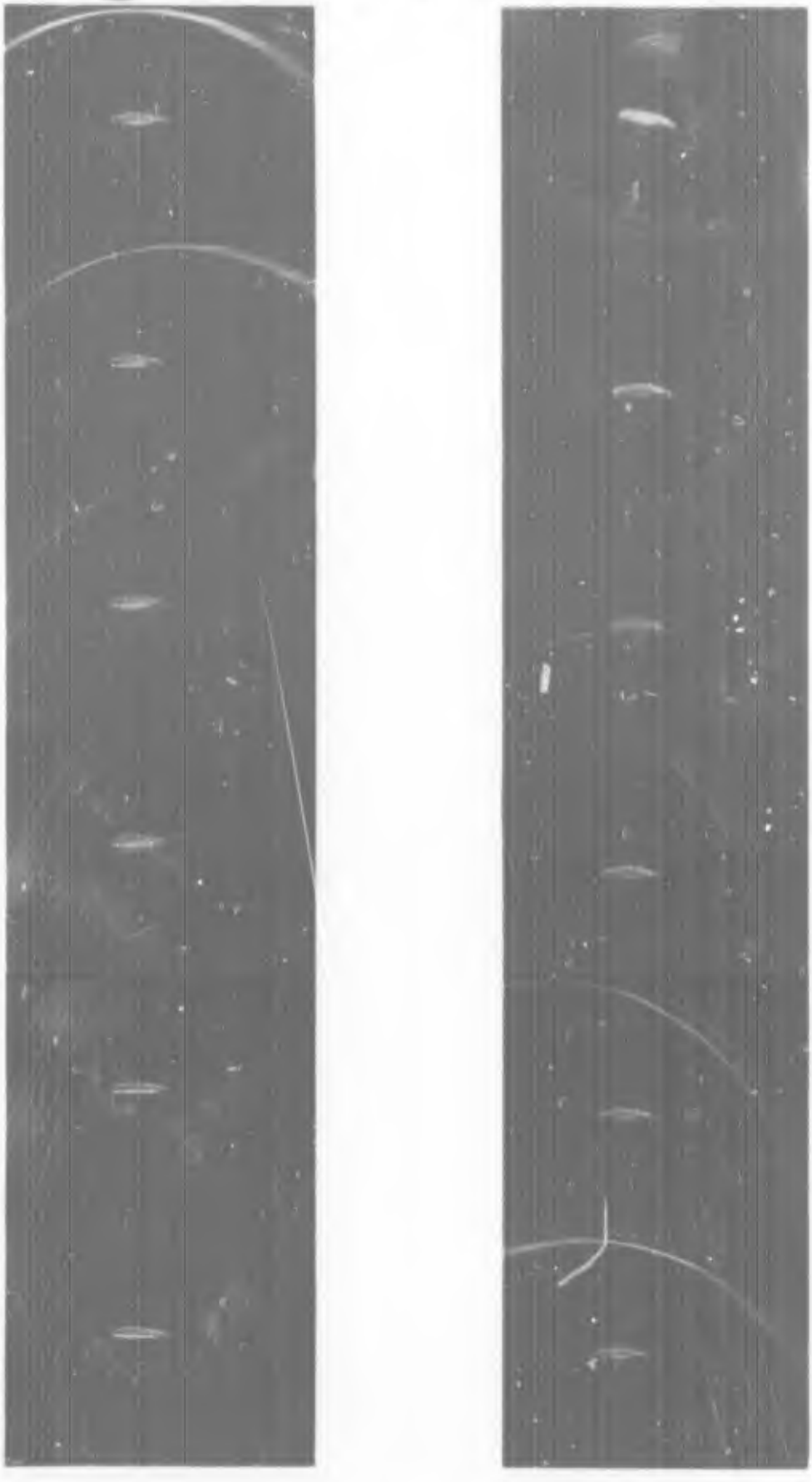

Figure 26 - One Cycle - J=0.56 - x/ℓ=0.5 Articulated Camera

Figure 27 - One Cycle - J=1.75 - x/L=0.5 Articulated Camera

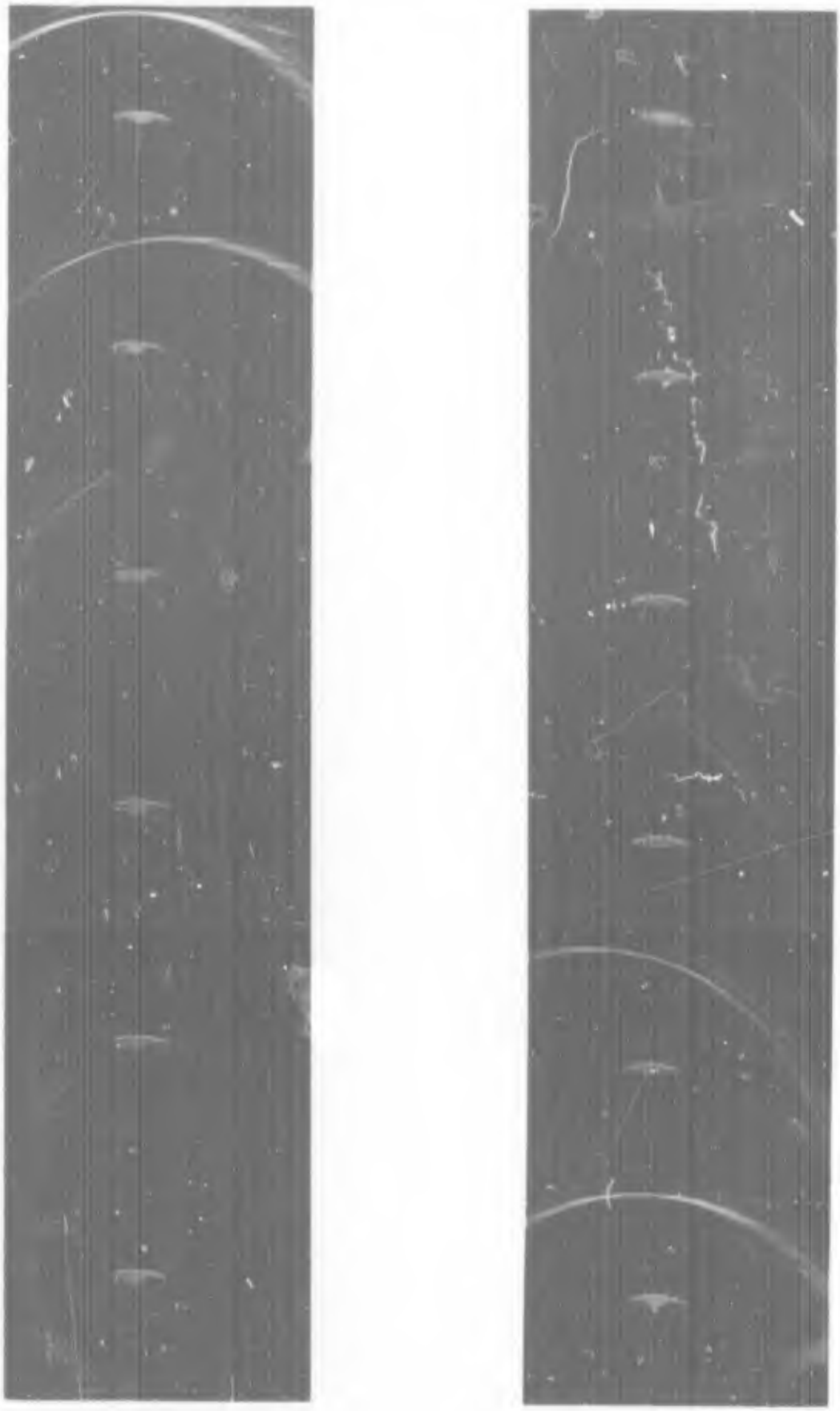

Figure 28 - One Cycle - J=3.50 - x/L=0.5 Articulated Camera

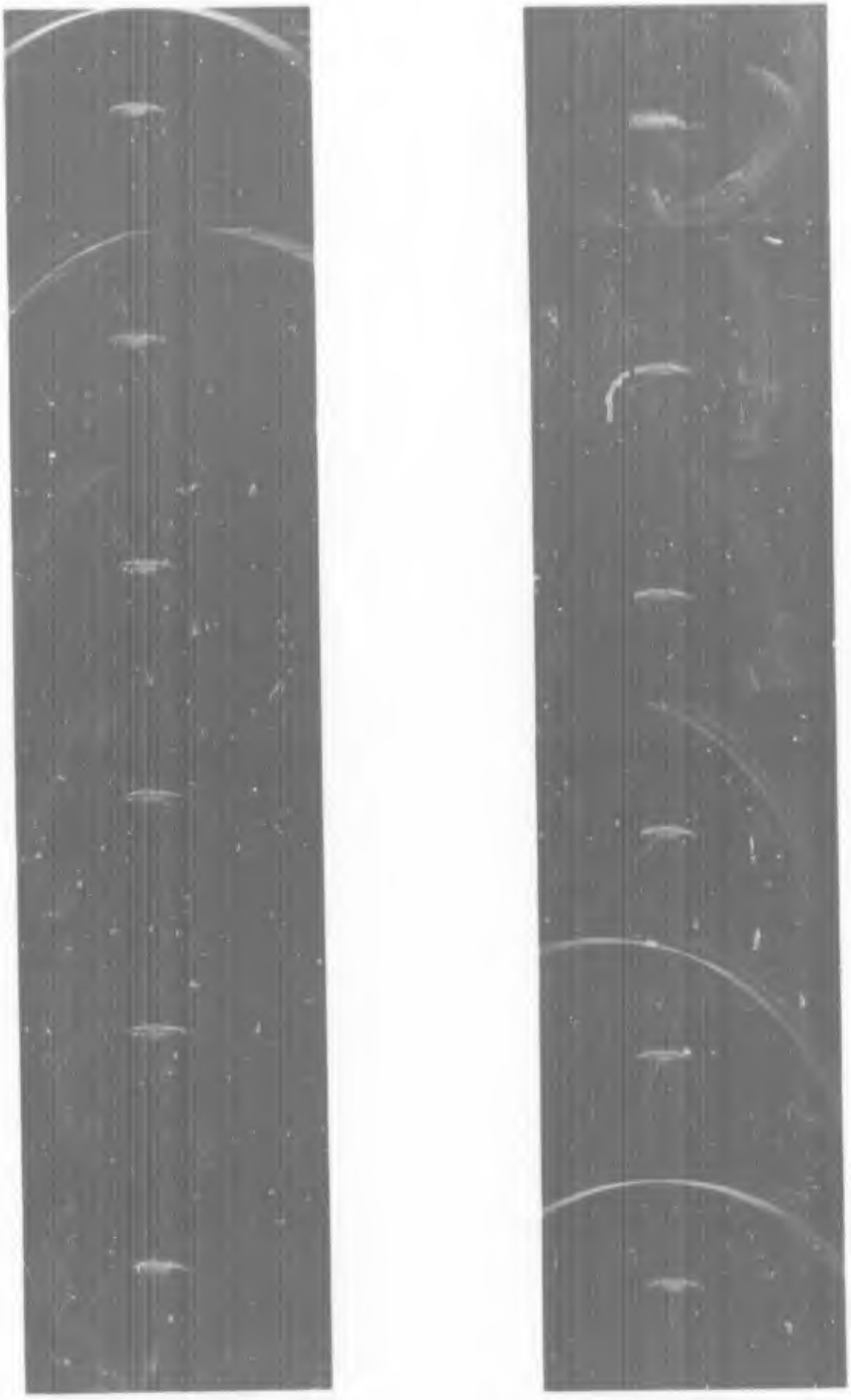

Figure 29 - One Cycle - J=4,50 - x/L=0.5 Articulated Camera

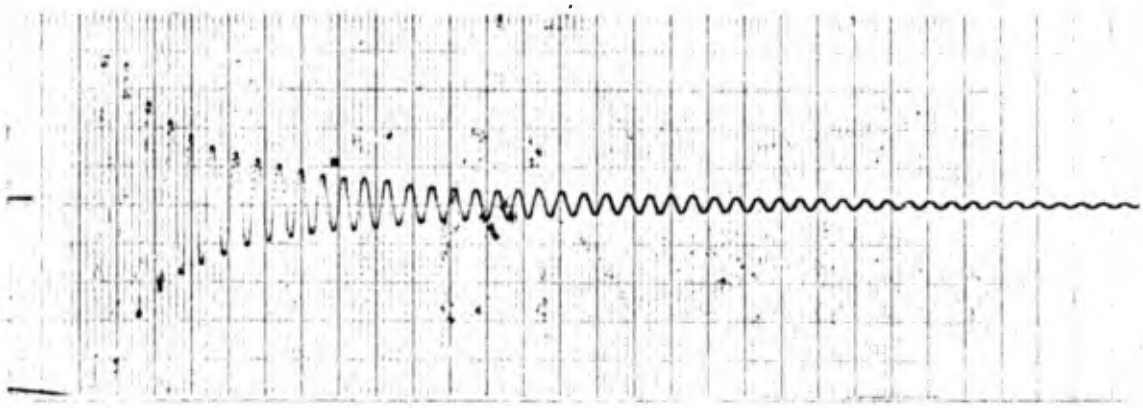

Natural Frequency of Blade and Blade Support - Model in Water -

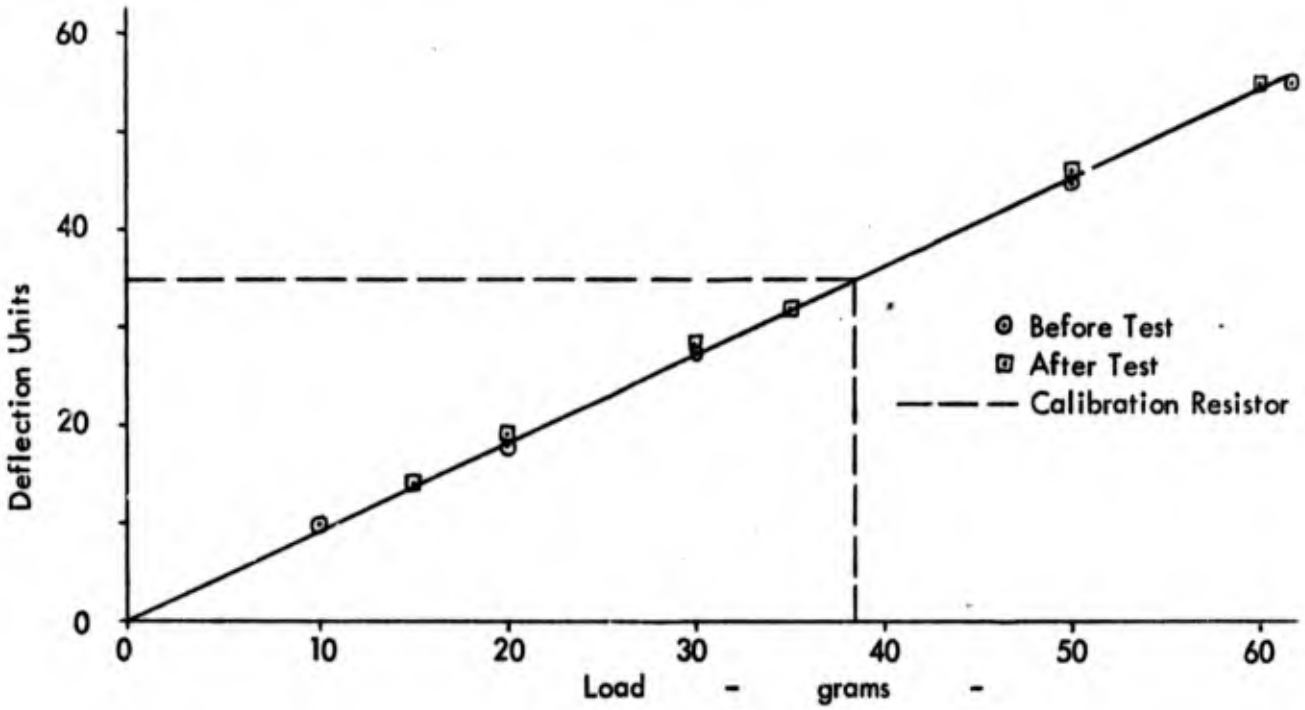

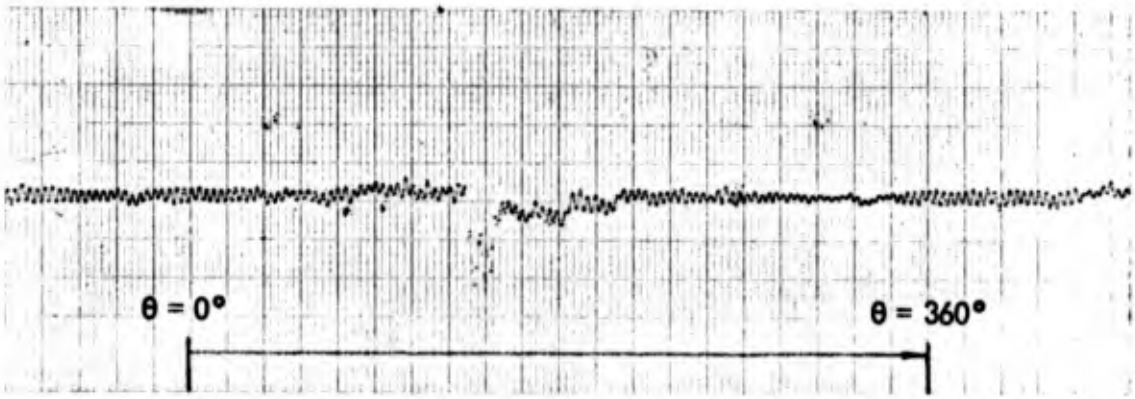

Inertia and Centrifugal Forces - Model in Air -

Figure 30 - Calibration and Inertia Data

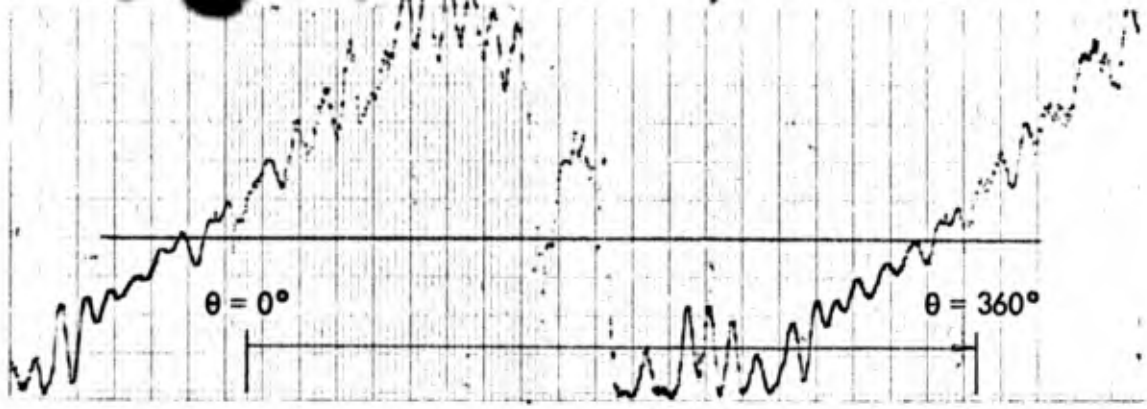

Blade Load - J = 0.56 -

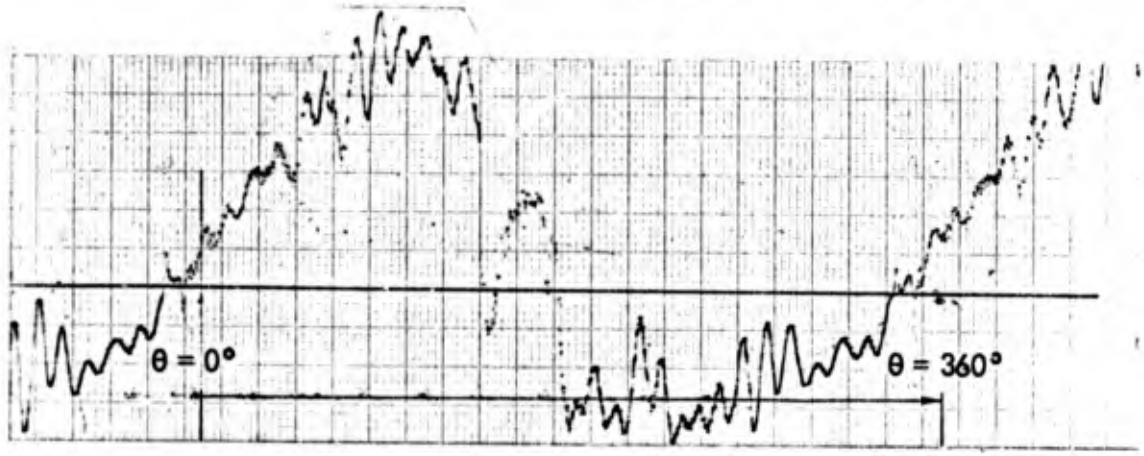

Blade Load - J = 1.75 -

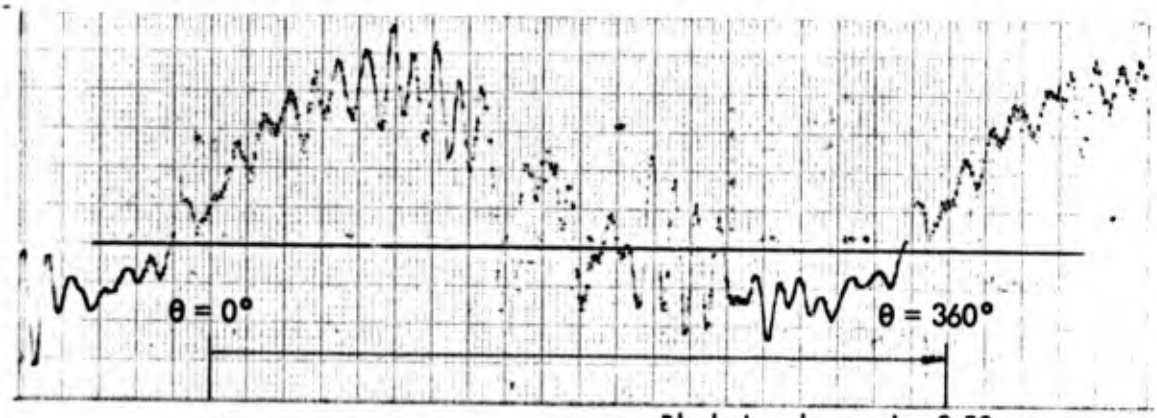

Blade Load - J = 3.50 -

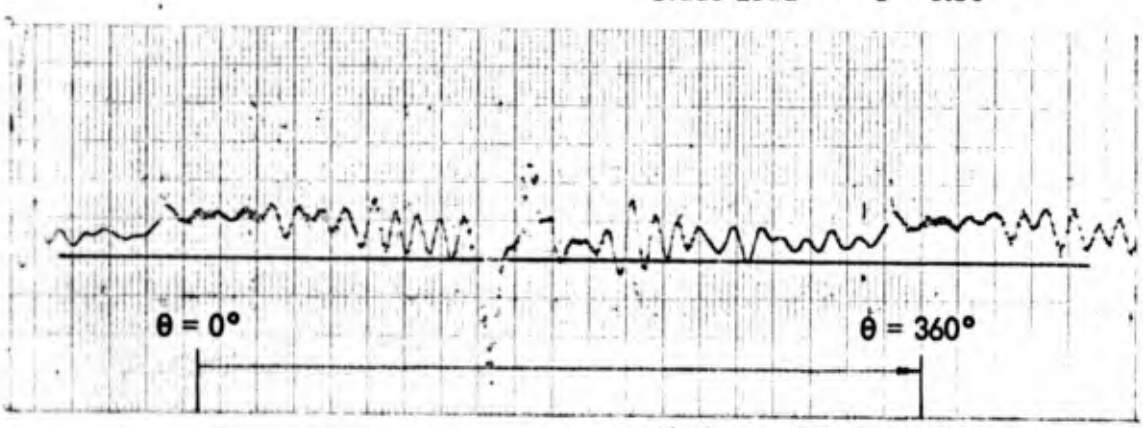

Blade Load - J = 4.50 -

Figure 31 - Blade Load Records

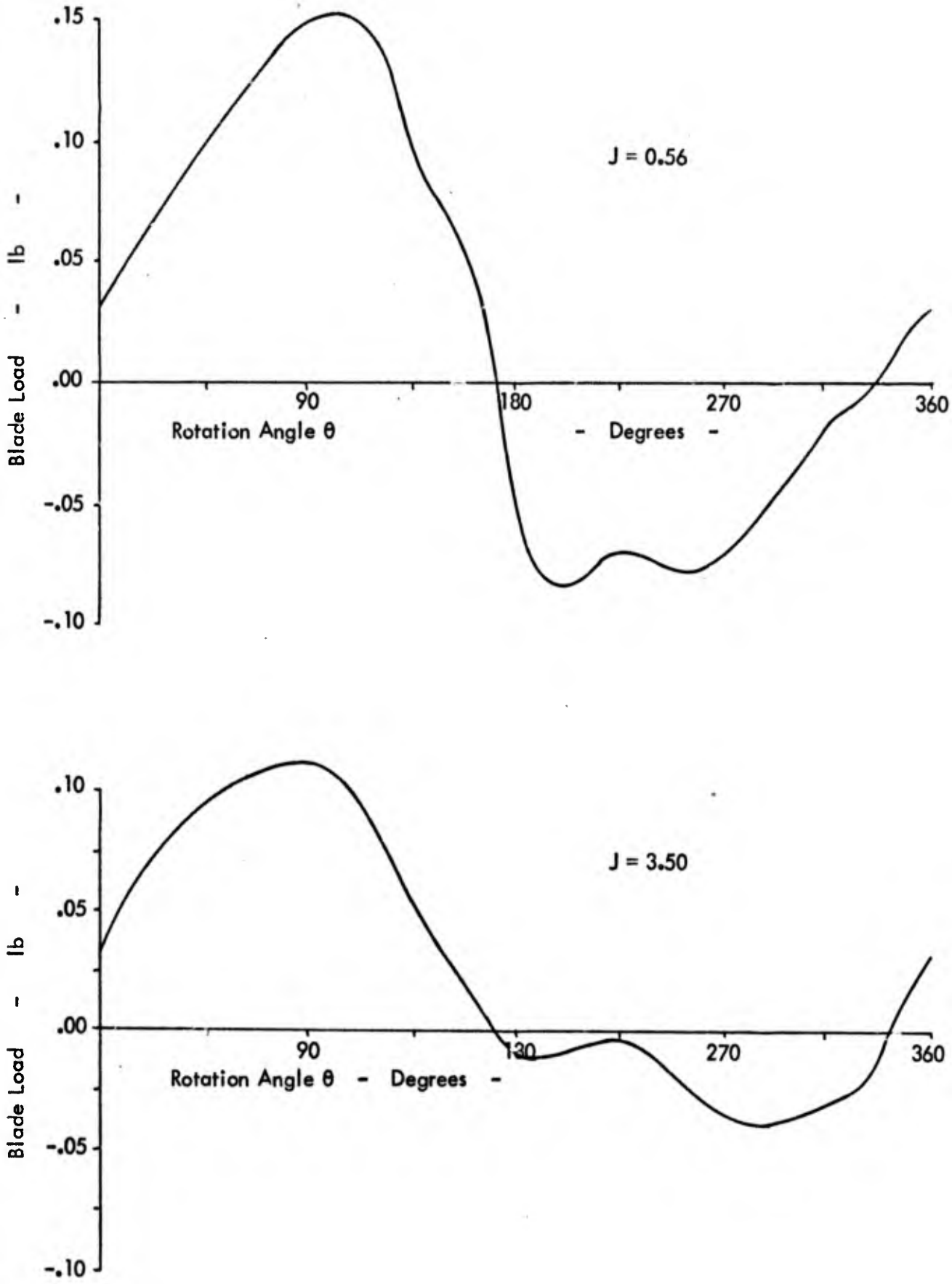

Figure 32 - Measured Blade Load - J = 0.56 and J = 3.50

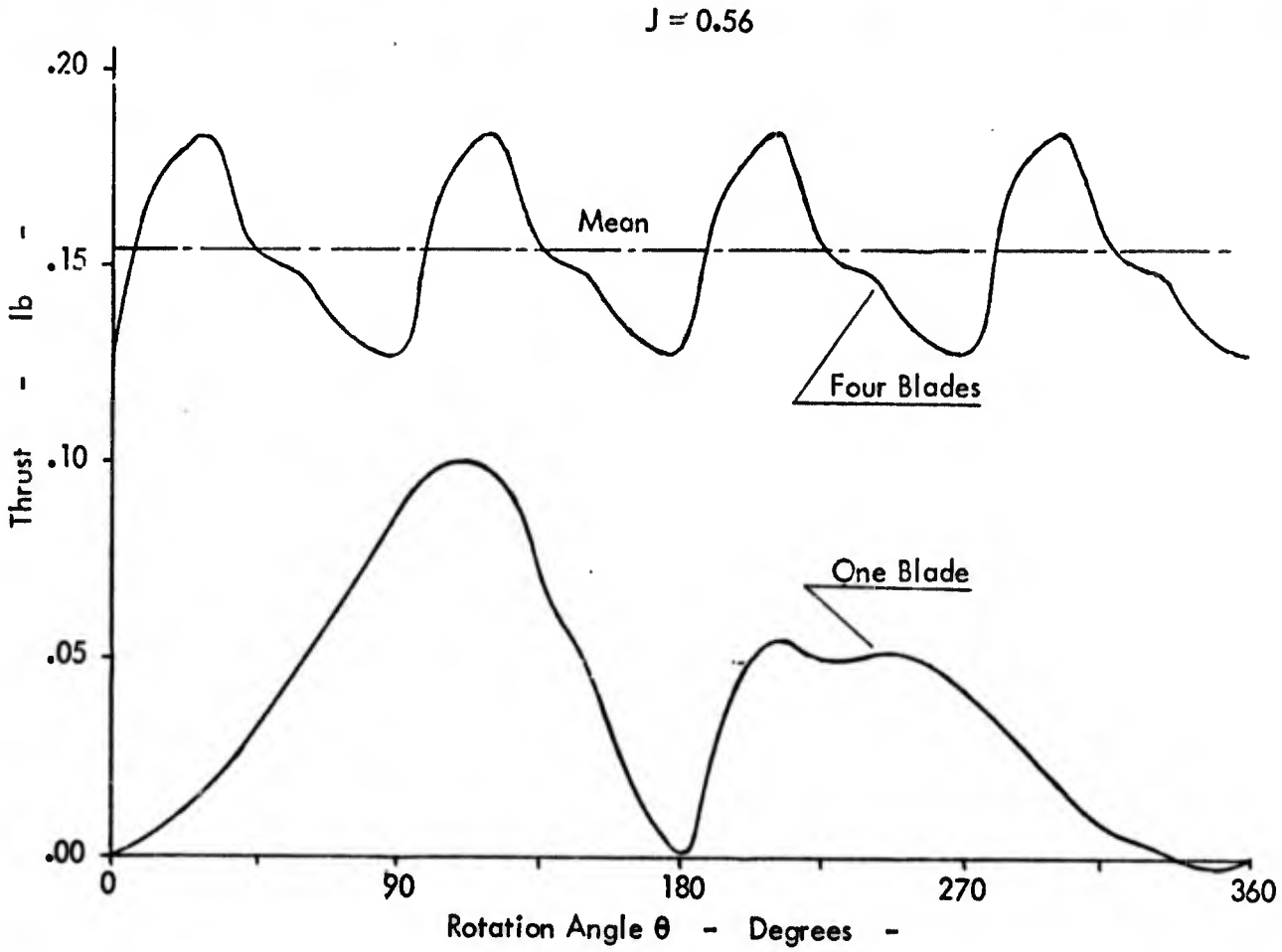

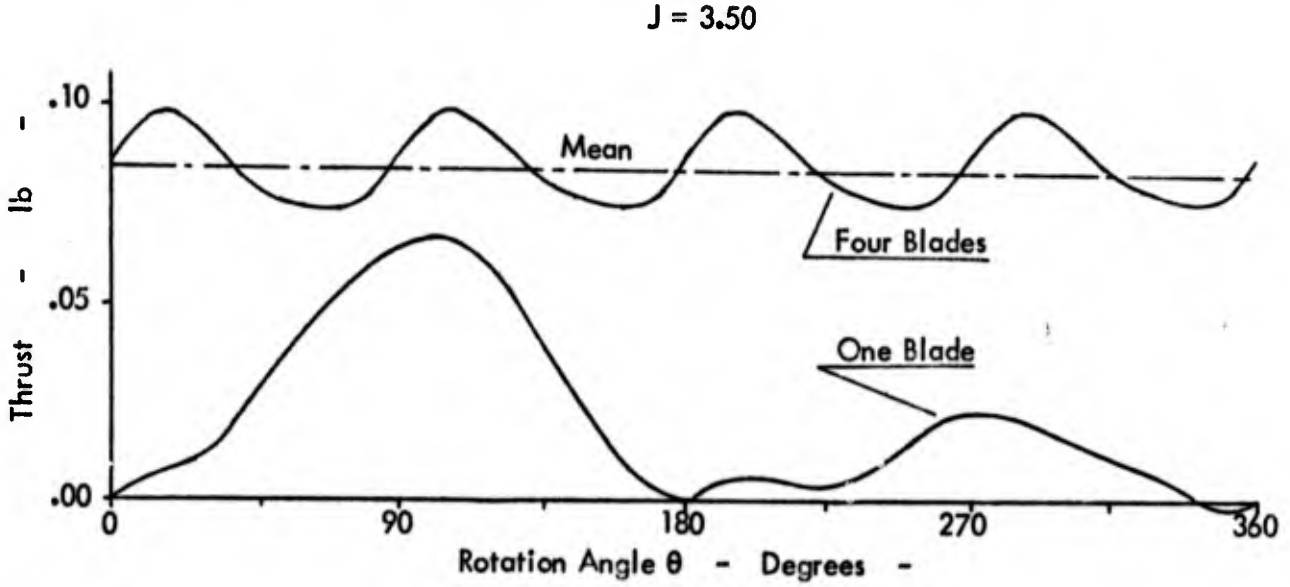

Figure 33 - Thrust Derived from Blade Load - J = 0.56 and J = 3.50

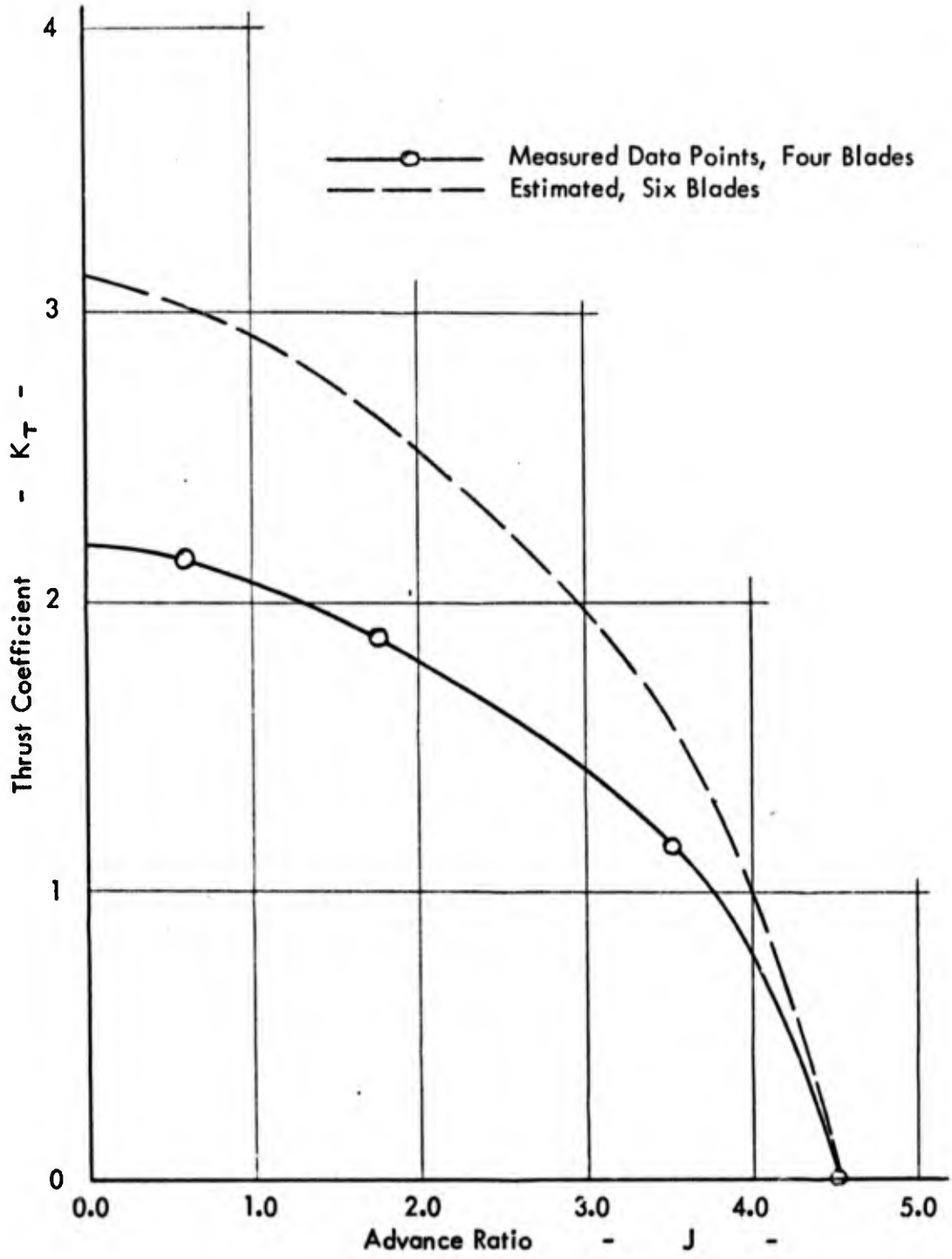

Figure 34 - Thrust Coefficient vs Advance Ratio

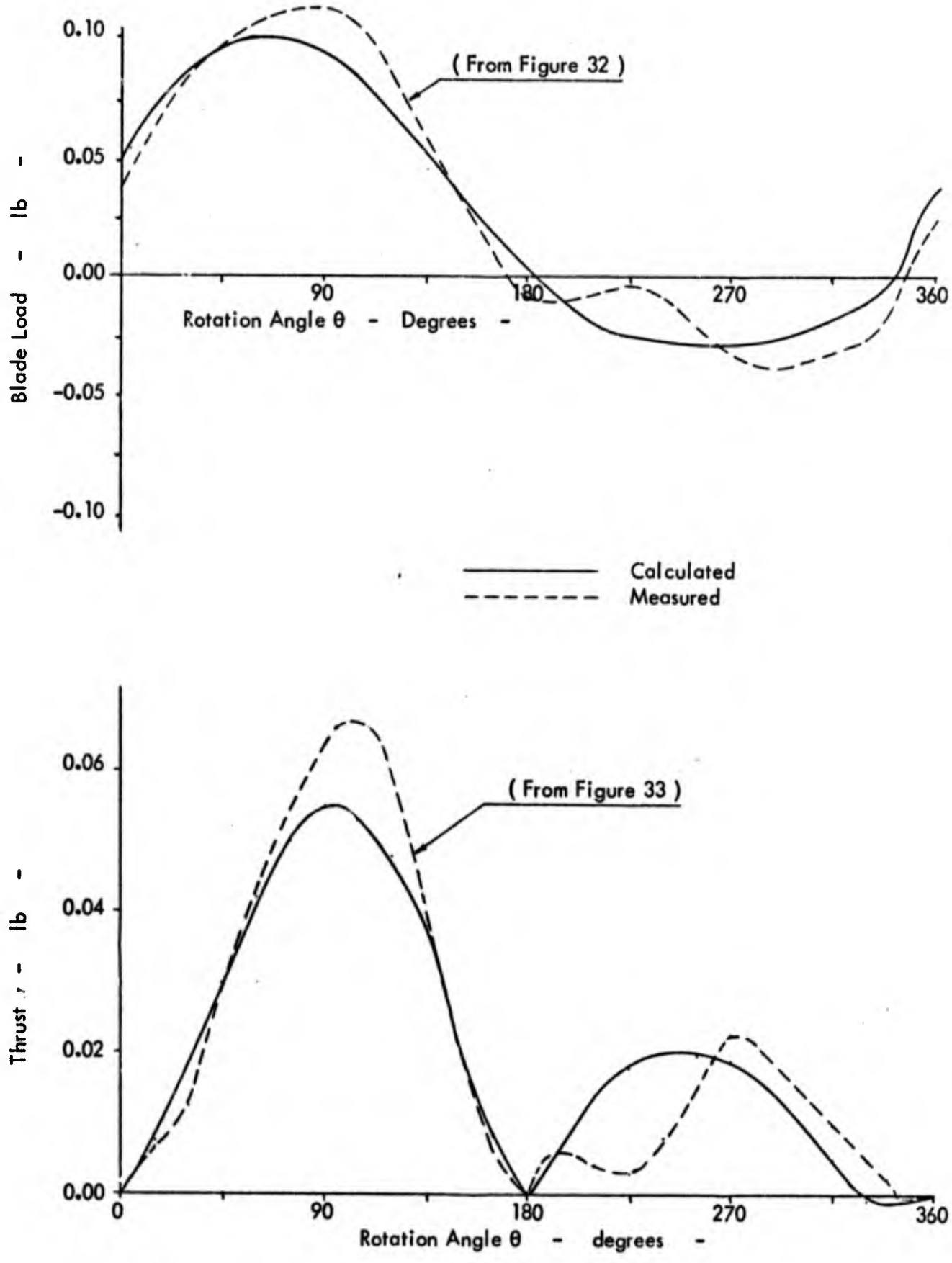

Figure 35 - Calculated Blade Load and Thrust vs. Measured Data - J = 3.50